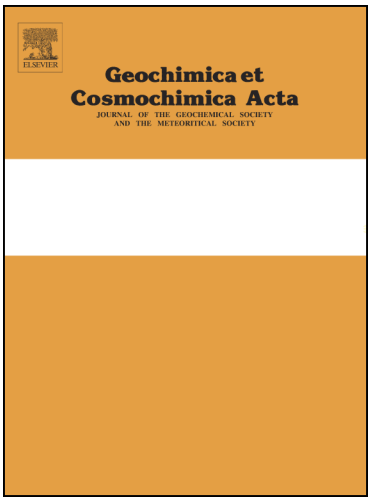


# Radiogenic isotopes in enriched mid-ocean ridge basalts from explorer ridge, northeast pacific ocean

Brian Cousens, Dominique Weis, Marc Constantin, Steve Scott

PII: S0016-7037(17)30381-2
DOI: http://dx.doi.org/10.1016/j.gca.2017.06.032
Reference: GCA 10345

To appear in: *Geochimica et Cosmochimica Acta*

Received Date: 27 April 2016
Revised Date: 31 May 2017
Accepted Date: 21 June 2017

Please cite this article as: Cousens, B., Weis, D., Constantin, M., Scott, S., Radiogenic isotopes in enriched mid-ocean ridge basalts from explorer ridge, northeast pacific ocean, *Geochimica et Cosmochimica Acta* (2017), doi: http://dx.doi.org/10.1016/j.gca.2017.06.032

# RADIOGENIC ISOTOPES IN ENRICHED MID-OCEAN RIDGE BASALTS FROM EXPLORER RIDGE, NORTHEAST PACIFIC OCEAN

Brian Cousens, Ottawa-Carleton Geoscience Centre, Isotope Geology and Geochronology Research Centre, Department of Earth Sciences, Carleton University, 1125 Colonel By Drive, Ottawa, ON. K1S 5B6, Canada

Dominique Weis, Pacific Centre for Isotope and Geochemical Research, Department of Earth, Ocean and Atmospheric Sciences, The University of British Columbia, 2020-2207 Main Mall, Vancouver, BC. V6T 1Z4, Canada.

Marc Constantin, Département de géologie et génie géologique, Université Laval, 1065 Ave de la Médecine, Québec, QC. G1V 0A6, Canada.

Steve Scott, Department of Earth Sciences, University of Toronto, 22 Russell Str., Toronto, ON. M5S 3B1, Canada.

ABSTRACT

Extreme gradients in topography related to variations in magma supply are observed on the Southern Explorer Ridge (SER), part of the northern Juan de Fuca ridge system. We report radiogenic isotope (Pb, Sr, Nd, Hf) and geochemical data for twenty-four basalt whole-rock and glass samples collected from the length of the SER and from Explorer Deep, a rift to the north of the SER. Lavas from the SER form a north-south geochemical gradient, dominated by E-MORB at the northern axial high, and range from T-MORB to N-MORB towards the southern deepest part of the ridge. Linear relationships between incompatible element ratios and isotopic ratios in MORB along the ridge are consistent with mixing of magmas beneath the ridge to generate the geographic gradient from E- to N-MORB. The E-MORB have high Sr and Pb, and low Nd and Hf isotopic ratios, typical of enriched mantle that includes a FOZO or HIMU isotopic

component. The West Valley and Endeavour segments of the northern Juan de Fuca ridge also include this isotopic component, but the proportion of the FOZO or HIMU component is more extreme in the SER basalts. The FOZO or HIMU component may be garnet-bearing peridotite, or a garnet pyroxenite embedded in peridotite. Recycled garnet pyroxenite better explains the very shallow SER axial high, high Nb/La and La/Sm, and the "enriched" isotopic compositions.

## 1. INTRODUCTION

The radiogenic isotope and incompatible element characteristics of mid-ocean ridge basalts (MORB) yield information on geochemical heterogeneity in the uppermost mantle and the presence of enriched components in the MORB mantle source. In many cases, heterogeneity in MORB is due to the presence of a mantle plume in proximity to a ridge that provides a flow of enriched mantle to the nearest ridge segments (e.g., Le Roex et al., 1992; Rhodes et al., 1990; Schilling, 1973, 1991; Schilling et al., 1983; White and Schilling, 1978). However, several studies have shown that, far from plume influences, adjacent mid-ocean ridge segments are commonly geochemically distinct from each other, indicating that the composition of the upper mantle and melting processes differ at length scales down to <100 km (e.g., Andres et al., 2004; Cousens, 2010; Gill et al., 2016; Hoernle et al., 2011; Macdougall and Lugmair, 1985; Niu et al., 1999; Salters et al., 2011; Thompson et al., 1985; Waters et al., 2011; Wendt et al., 1999). Although many subdivisions in mid-ocean ridge basalt (MORB) chemical types have been proposed, ratios of incompatible trace elements are commonly used to classify MORB as depleted or normal (N-), transitional (T-), and enriched (E-) types. Typically, primitive mantle-normalized ($_N$) values for either La/Sm or Nb/Zr are < 0.8, 0.8 to 1.2, and >1.2 in N-, T-, and E-MORB, respectively. Several authors use the ratio of $K_2O/TiO_2$ as a measure of enrichment of basalts in incompatible elements, since more basalts are analyzed for major element than for trace element abundances (e.g., Gill et al., 2016; Michael et al., 1989). N-MORB have ratios < 0.15, T-MORB are between 0.15 and 0.25,

and E-MORB have ratios > 0.25. Gill et al. (2016) also define highly depleted D-MORB with $K_2O/TiO_2 < 0.07$.

The Juan de Fuca ridge system along the west coast of North America is the remnant of the Farallon-Pacific plate boundary (Atwater, 1970; Atwater and Stock, 1998; Botros and Johnson, 1988; Caress et al., 1988; Menard, 1978; Riddihough, 1984). As the size of the Farallon plate has diminished over the past 150 Ma and the Farallon-Pacific spreading centre has reached the North American margin, the former Farallon plate has broken up into the Gorda, Juan de Fuca, and Explorer plates (Riddihough, 1984; Wilson et al., 1984). Due to the proximity of the North American continental margin, ridge segmentation in the form of short transform faults, overlapping spreading centres, and pull-apart rifts are well developed at the north end of both the Juan de Fuca and Explorer ridges (Figure 1A) (Davis and Currie, 1993; Rohr and Furlong, 1995). These features are likely the result of very rapid ridge reorientation (clockwise rotation) and ridge "jumps" through the late Cenozoic (Botros and Johnson, 1988; Dziak, 2006; Rohr and Furlong, 1995).

Previous geochemical studies of the Juan de Fuca ridge system have shown that it can be split into two geochemical provinces separated by the Cobb Offset, a small overlapping spreading centre in the north-central Juan de Fuca ridge (Figure 1A, inset). To the south of the Cobb Offset are the Gorda and southern Juan de Fuca ridges, characterized by N- and T-type MORB (Chadwick et al., 2005; Dixon et al., 1986; Dreyer et al., 2013; Rhodes et al., 1990; Smith et al., 1994). North of the Cobb Offset, the northern Juan de Fuca ridge, Explorer, and Tuzo Wilson segments are composed of E-, T- and N-type MORB (Figure 2) (Allan et al., 1993; Bjerkgard et al., 2000; Cousens et al., 1995; Cousens et al., 1984; Gill et al., 2016; Karsten et al., 1990; Kelley et al., 2012; Michael et al., 1989; Stakes and Franklin, 1994; Van Wagoner and Leybourne, 1991; Woodcock et al., 2006).

Remarkably, there are few comprehensive radiogenic isotopic data available for MORB erupted along the Juan de Fuca system (Cousens et al., 1995; Davis et al., 2008; Gill et al., 2016; Hegner and Tatsumoto, 1987; Salters et al., 2011), although some Juan de Fuca basalts have been analyzed for one or more isotopes as part of regional studies (Church and Tatsumoto, 1975; Eaby et al., 1984; Lupton et al., 1993; White et al., 1987)

or at Axial Seamount (Chadwick et al., 2005; Rhodes et al., 1990). Here we report new major element and trace element concentrations in 49 basalt glass and whole-rock samples from Explorer Ridge and Pb-Sr-Nd-Hf isotopic data for a subset of 24 of the samples. Our new data further document the importance of enriched components in the upper mantle beneath Explorer Ridge. We compare the composition of the Explorer enriched component with that observed in other mid-ocean ridge segments and seamounts in the Northeast Pacific, in order to evaluate the breadth in the mantle over which the enriched components may be distributed.

## 2. LOCAL GEOLOGY

The former Farallon plate now consists of the Gorda, Juan de Fuca, and Explorer plates (Figure 1A, inset) (Riddihough, 1984; Wilson et al., 1984). The Sovanco fracture zone, which links the northern segments of the Juan de Fuca Ridge to Explorer Ridge, formed at approximately 7.4 Ma and lengthened rapidly as Explorer Ridge shifted to the northwest (Botros and Johnson, 1988). However, the Explorer plate has only been independent from the Juan de Fuca plate since ca. 4 Ma when the Nootka Fault was initiated (Botros and Johnson, 1988; Riddihough, 1984). The orientation of Explorer Ridge has since rotated clockwise by a number of rift propagation events and an eastward ridge jump during the last 0.7 Ma. Thus the modern Explorer Ridge consists of three segments: the more robust Southern Explorer Ridge (SER), the Explorer Deep rift to the northeast, and a complex set of en-echelon rifts to the northwest termed Northern Explorer Rifts (Botros and Johnson, 1988; Embley, 2002). The latter two rifts terminate along the Revere-Dellwood fracture zone (Figure 1A). On the northeast side of the Revere-Dellwood fracture zone, pull-apart rifting has been identified at the Dellwood Knolls (Bertrand, 1972; Riddihough et al., 1980) and at the Tuzo Wilson volcanic field (Allan et al., 1993; Carbotte et al., 1989).

Multibeam bathymetry and side-scan sonar surveys in the early 1980's demonstrate that the SER is in a period of sustained high magma supply, with a minimum depth of only 1750 m near its northern end (the axial high) that tapers to a depth of > 2400 m at its south end (Kappel and Ryan, 1986). A narrow central rift that disappears at the

shallowest part of the ridge cuts the SER. In 2002, NOAA conducted an EM300 and deep-tow (ABE) bathymetric survey of the northern half of the SER as well as the Northern Explorer Rifts and Explorer Deep as part of a study of hydrothermal activity along the ridge, largely at the Magic Mountain field (Figure 1B) (Embley, 2002; National Oceanic and Atmospheric Administration, 2002b; Scott et al., 1990; Tunnicliffe et al., 1986).

Explorer Seamount, located on the west side of a deep trough at the south end of SER, rises to a water depth of 870 m (Chase et al., 1982). Chase et al. (1982) concluded that Explorer Seamount is ca. 4.5 Ma in age and originated near the Juan de Fuca ridge as a near-ridge seamount. However, further analysis of the magnetic anomaly patterns indicated that the southeastern peak of Explorer Seamount is of Brunhes epoch age (< 0.78 Ma) (Mingxian et al., 1986). SeaBeam mapping of Explorer Seamount shows that it is composed of a series of north-south oriented curvi-linear ridges (Davis and Currie, 1993), rather than more point-source volcanic edifices typical of near-ridge seamount chains (e.g., Dellwood seamounts, Figure 1A, (Davis and Currie, 1993)). The young magnetic ages from Explorer Seamount indicate that it was produced at the south end of Explorer Ridge (Mingxian et al., 1986) and is therefore part of the Explorer spreading system. If so, then the extremely shallow water depth of the main peak requires that it has been uplifted by post-eruption deformation at the south end of the spreading ridge.

Structural and seismicity studies suggest that Explorer Plate is unstable, and plate deformation is consistent with the initiation of a new, broad Pacific-Juan de Fuca transform boundary that cuts across the Explorer and Pacific plates from the southern end of the Queen Charlotte Islands to the northern Juan de Fuca Ridge (Dziak, 2006; Rohr and Furlong, 1995). If so, then at some point in the future all spreading on Explorer Ridge will cease and most of the Explorer Plate will merge with the North American Plate.

Most of the basalt samples from the SER were collected around the Magic Mountain hydrothermal vent field, located on the shallowest section (axial high) of the SER (Figure 1B) (Embley, 2002; National Oceanic and Atmospheric Administration, 2002a; Tunnicliffe et al., 1986). The Explorer Ridge segments north and south of Magic

Mountain have not been investigated by well-navigated submersible or remotely-operated vehicle surveys and remain poorly studied (Cousens et al., 1984; Michael et al., 1989).

## 3. SAMPLE COLLECTION AND ANALYTICAL TECHNIQUES

Samples from Explorer Deep, the SER and Explorer Seamount are from the University of British Columbia (UBC) dredge collection, including research cruises from 1979 to 1995, augmented by a set of samples from the SER retrieved during two University of Toronto (UT) cruises in 1994 and 1995 (CR3 and CR4) and a NOAA Ocean Exploration cruise in 2002 (TN149, Embley, 2002; National Oceanic and Atmospheric Administration, 2002a) (Figure 1B).

The UBC samples include glass separates and whole-rock powders from dredge hauls or camera sled tows whereas UT samples were collected by ROV *ROPOS* or camera sled tows. The glasses are fresh and commonly plagioclase-phyric. The crystalline pillow interiors are generally aphyric but may include plagioclase, olivine and rare pyroxene phenocrysts in a microcrystalline groundmass. Samples CR2-D39-1, CASM3-1, CR3-D281-05, CR4-CV35-01, CU1-D13-01, AND CASM5-D11 are highly (up to 20%) plagioclase-porphyritic basalts with lesser amounts of olivine and pyroxene phenocrysts.

Samples obtained during the 2002 NOAA cruise include six glass samples collected using a rock coring apparatus (samples "RC") (e.g., Reynolds et al., 1992) and four fragments of pillow and sheet lavas collected by ROV *ROPOS*. Rock core casts were precisely located using GPS and the EM300 bathymetric system on the RV *Thomas G. Thompson*, and individual casts recovered between 1.5 and 8.0 grams of glass. Four out of six rock core sites were on the Seminole Ridge (SR in Figure 1B) of the SER (Michael et al., 1989), a shallow ridge that parallels the SER on its east side between 49°44'N and 49°48'N. The origin of this ridge is uncertain, and has been proposed to be either a propagating ridge or a seamount. Sample RC-01 was the only rock core sample to have mud smeared in the wax-filled cutters along with fresh glass, and thus this large seamount on the east side of the Seminole Ridge is possibly older than features sampled at the other 3 rock core stations. Sample R665-RK-0029, from the central rift valley, is a fine-grained basalt with a thick glassy rind that includes 15% plagioclase phenocrysts in the glass. Whole-rock sample R667-RK-0001 is a porphyritic basalt, collected from a pancake-

shaped volcanic feature on the west side of the central rift, that includes 15% blocky plagioclase crystals up to 3mm in size in a fine-grained matrix. Whole-rock sample R670-RK-0016 is a pillow fragment, collected from the base of a hydrothermal vent structure, with an aphyric, vesicular texture. Sample R668-RK-0005gl is the glassy rind of a vesicular, chloritized basalt, also collected from the base of a hydrothermal vent structure. All whole-rock samples included a thin veneer of Fe-Mn oxides, with fresh to mildly chloritized interiors.

Previous studies of E-MORB on the East Pacific Rise has suggested that E-MORB were primarily erupted off-axis (e.g., Perfit et al., 1994), but recent work shows that the E-MORB lavas recovered in earlier studies are in fact long lava flows that originated from the ridge axis (Waters et al., 2011). During the 2002 NOAA cruise to Explorer Ridge, the EM300 acoustic backscatter data suggested that a lava flow in Explorer Deep actually originated from a small cone on the North SER region and flowed at least 10 km downslope. Thus, E-MORB pillow basalts recovered in dredge 79-06-32 from Explorer Deep, collected in 1979 prior to either SeaBeam or EM300 surveys, potentially came from a long lava flow that originated from the SER. However, the dredge haul track includes a scarp and a small volcanic platform that are adjacent to at least two prominent volcanic cones that are clearly distinguished in the EM300 bathymetric and backscatter data, and are at the correct depth range to have been the target of the dredge (2375-2465 m).

Fresh, oxide-free glass fragments and rock chips were washed in distilled water to remove salts and crushed in an agate mortar. Major element oxide concentrations were determined were by electron microprobe at the University of Toronto (UBC and UT glasses) and Carleton University (NOAA glasses) and by fused-disc X-ray fluorescence spectrometry at the University of Ottawa (NOAA whole-rocks). The UBC/UT glasses and whole-rock powders were analyzed for select trace elements by instrumental neutron activation analysis (INAA) and inductively coupled-plasma (ICP) techniques at the University of Toronto (techniques from Michael et al., 1989; Stix and Gorton, 1992), whereas glasses and whole-rock samples from the NOAA cruise were analyzed for trace elements by inductively coupled plasma-mass spectrometry (ICP-MS) at the Ontario Geological Survey. Major and trace element data are listed in Table 1, along with

analytical precision estimates based on analysis of international standards and blind standards included in all runs.

Based on a comparison of the trace element compositions of basalts from the Axial High determined by ICP-MS and INAA, we note that there are some consistent discrepancies between the data sets. At a given La content, the INAA analyses yield Ta, Yb, and Sm values higher by ~ 10% than the ICP-MS analyses. Other trace elements (Ce, Nd, Tb, Y, Th, Nb) generally overlap in the two data sets, and the differences are not obvious in Primitive Mantle-normalized incompatible element patterns. These consistent differences have an impact on La/Sm and especially on Tb/Yb ratios that are discussed in the text and plotted in figures. The raw data are listed in the data tables, but Yb values determined by INAA and used in ratios plotted in figures have been corrected so as to be comparable to the ICP-MS Yb data. Y concentrations are highly comparable between the two data sets, so the correction to Yb was accomplished using the following equation:

$$Yb_{corr} = (Y*0.09421)+0.06782$$

where Y is the yttrium concentration in parts per million. In all figures using this correction, the caption will indicate that the corrected value of Yb was used in the calculation of the ratio in the figure.

In their electron microprobe and laser-ablation ICP-MS study of basaltic glasses in the Smithsonian collection, Jenner and O'Neill (2012a, 2012b) report major and trace element analyses of samples from SER, the Seminole Ridge, and Explorer Seamount. One of these glass samples, from Explorer Seamount, was also analyzed for its Sr isotopic composition (Hegner and Tatsumoto, 1989). Data from these analyses have been incorporated into this study (sample locations in Figure 1B). In addition to samples from the ridge segments listed above, Jenner and O'Neill (2012b) present analyses from the elevated ridge along the southeast flank of SER, termed "30´-Ridge" by Michael et al. (1989), that are also included in this study (Figure 1B).

The UBC/UT and NOAA samples were analyzed for Pb, Sr, and Nd isotopic ratios by Finnigan-MAT261 and Thermo-Finnigan Triton T1 thermal ionization mass spectrometers (TIMS) at Carleton University (techniques of Cousens, 1996). Splits of the

sample powders for Sr isotopes were acid-washed in hot 6N HCl for three to five days prior to dissolution to remove Sr added to the rocks from seawater. Even so, two glass samples (RC-02 and R668-RK0005gl) have $^{87}Sr/^{86}Sr$ that are slightly high given their $^{143}Nd/^{144}Nd$. Pb mass spectrometer runs for the NOAA rocks were performed on the MAT261 and were corrected for fractionation using NIST SRM981. The average ratios measured for SRM981 are $^{206}Pb/^{204}Pb = 16.889 \pm 0.011$, $^{207}Pb/^{204}Pb = 15.426 \pm 0.012$, and $^{208}Pb/^{204}Pb = 36.495 \pm 0.042$ (n=45, 1999-2003). The Pb fractionation correction is +0.15% per amu (based on the SRM981values of Galer and Abouchami, 1998). Sr and Nd isotope ratios were measured on both mass spectrometers, and all analyses are reported relative to the standard values reported below. Sr isotope ratios are normalized to $^{86}Sr/^{88}Sr = 0.11940$. Two Sr standards were run at Carleton from 1999 to 2003, NIST SRM987 ($^{87}Sr/^{86}Sr = 0.710256 \pm 19$, n=35) and the Eimer and Amend (E&A) $SrCO_3$ ($^{87}Sr/^{86}Sr = 0.708023 \pm 12$, n=14). Nd isotope ratios are normalized to $^{146}Nd/^{144}Nd = 0.72190$. Analyses of the USGS standard BCR-1 yield $^{143}Nd/^{144}Nd = 0.512668 \pm 20$ (n=4), and 15 runs of the La Jolla standard average $^{143}Nd/^{144}Nd = 0.511867 \pm 15$. All quoted uncertainties are 2-sigma standard deviations of the mean.

A subset of the UBC rock powders were run for Pb and Hf isotopes utilizing a Nu Instruments 021 multicollector ICP-MS (following the procedures of Weis et al., 2007; Weis et al., 2006) and after careful leaching (Nobre Silva et al., 2009; Nobre Silva et al., 2010). The mean Pb isotope values for NBS981 obtained during the three-day analysis period were $^{206}Pb/^{204}Pb = 16.9412 \pm 0.0013$, $^{207}Pb/^{204}Pb = 15.4961 \pm 0.0015$, and $^{208}Pb/^{204}Pb = 36.7133 \pm 0.0040$ (n=28). International standard BHVO-1 was run during the analysis period, and yielded $^{208}Pb/^{204}Pb = 38.3886$ +/- 0.0074, $^{207}Pb/^{204}Pb = 15.5795$ +/- 0.0029, and $^{206}Pb/^{204}Pb = 18.6983$ +/- 0.0025. Hf isotope ratios were corrected for instrument fractionation using $^{179}Hf/^{177}Hf = 0.7325$. The JMC475 standard yielded a mean $^{176}Hf/^{177}Hf$ of $0.282159 \pm 0.000010$. The Explorer samples were run during the same time period that studies of USGS reference materials were conducted at UBC, and the data and precision estimates for BHVO-1 are documented in Weis et al. (2005) (2006). All isotopic data are listed in Table 2.

## 4. RESULTS

*4.1 Major and Trace Elements*

The glasses and whole-rock samples from Explorer Ridge and Explorer Seamount are all subalkaline basalts. Mg#'s range from 0.64 to 0.51 in SER glasses and whole-rocks, 0.69 to 0.58 in Explorer Deep glasses, and 0.65 to 0.62 in Explorer Seamount glasses. The SER samples fall into two groups in a plot of $K_2O$ vs. Mg# (Figure 3). The first group includes North and South SER lavas as well as six samples from the shallowest area on the ridge (Axial High and Seminole Ridge), with a maximum $K_2O$ content of 0.4% at a Mg# of 0.55. Most SER lavas from the axial high have higher $K_2O$, ranging from 0.36% (Mg# = 0.63) to 0.62% (Mg# = 0.53). These two groups are also evident in a plot of $K_2O/TiO_2$ vs. Mg#, where the low $K_2O$ lavas also have $K_2O/TiO_2 < 0.25$ (T-MORB) and the high $K_2O$ lavas have $K_2O/TiO_2$ between 0.27 and 0.35 (E-MORB). Explorer Deep glasses do not always fall in the SER trends in Figure 3. Sample 79-06-32-27, a vesicular glassy basalt, is a near-primary melt of the mantle with 9.91% MgO (dry basis), but has a low $CaO/Al_2O_3$ of 0.77 compared to the least evolved SER lavas. The other two Explorer Deep samples also have low $CaO/Al_2O_3$ compared to SER lavas of the same Mg#. Explorer Seamount glasses differ dramatically from the Explorer glasses: given their high Mg#, they have relatively low $K_2O$, $CaO/Al_2O_3$ and $K_2O/TiO_2$ (also CaO and $P_2O_5$, not shown), but high $Al_2O_3$ (16.8 – 17.3%) and $Na_2O$ (2.8 to 3.1%). Glasses from the 30´-Ridge are high in MgO compared to most SER basalts, are low-$K_2O$ T-MORB, and have low $CaO/Al_2O_3$ for their Mg#.

Like MgO, Cr (1170 ppm) and Ni (346 ppm) in Explorer Deep whole-rock sample 79-06-32-27 are near-primary magma concentrations (see also Michael et al., 1989). Sample 79-06-32-27 has large (centimeter-size) olivine crystals ($Fo_{92}$, NiO=0.31 wt %, possibly mantle xenocrysts) with numerous chromite inclusions, hence the high Cr and Ni concentrations (the major element composition of glass was obtained by electron microprobe and does reflect a near-primary magma composition). Cr and Ni in SER basalts, Explorer Seamount rocks and the other Explorer Deep sample are < 350 and < 180 ppm, respectively. Sc concentrations are lowest in the most MgO-rich lavas (~ 35 ppm), increase to 45-50 ppm in lavas with Mg#'s of 0.55, and then decrease in the more evolved lavas (not shown). In the SER lavas, concentrations of the incompatible

elements, including the REE (e.g., Ce, Figure 3; also Nd, Yb, Hf, Ta, Th, not shown), show an increase with decreasing Mg#, especially in the high-$K_2O$ group that consistently shows higher concentrations of these incompatible elements by a factor of 1.7 to 1.8. The more evolved sample from Explorer Deep, 79-06-32-42, has REE, Ba, Hf, Ta and Th contents (Table 1) that fall within the high-$K_2O$ group from SER. The most primitive Explorer Deep sample, 79-06-32-27, has Ce, Nd, Hf, Ta, Th and Ba concentrations that are low compared to the high-$K_2O$ SER group but fall close to an extension of a best-fit line through the high-$K_2O$, Axial High group. Explorer Seamount basalts typically have the lowest incompatible element abundances of the sample set.

Basalt glasses from different segments of the SER system commonly exhibit different $FeO^t$ and $Na_2O$ abundances at a given MgO content (Figure 4). Most of the SER samples form a broad negatively-sloping array typical of mid-ocean ridge segments world-wide (Klein and Langmuir, 1987, 1989). Different segments of the SER form subgroups around the best-fit line through the Axial High samples, consistent with some variation in primary magma compositions and in the liquid line of descent. Explorer Seamount glasses are distinctly enriched in both $FeO^t$ and $Na_2O$ compared to SER segments to the north, even though these relatively MgO-rich N-MORB are highly depleted in incompatible elements (Figure 3). The high $Na_2O$ and $FeO^t$ abundances are anomalous for N-MORB, and suggests that the source of these basalts includes some component other than depleted mantle peridotite.

Figure 5 shows Primitive Mantle (PM)-normalized (values of Sun and McDonough, 1989) incompatible element patterns for representative samples from this study. All Explorer Deep, SER North and SER Axial High samples are T- or E-MORB ($La/Sm_N$ = 1.5-2.3) with maximum PM-normalized values at Ta (and Nb, not shown). SER Axial High samples fall in two groups with parallel patterns, one with higher abundances of incompatible elements but large negative Sr anomalies and one with lower abundances that lack negative Sr anomalies. Since both glass and whole-rock analyses fall in each group, phenocryst abundance is not a first-order control on the split into the two groups (note glass and whole-rock trace element analyses for sample R665-RK-0029 are very similar, Table 1). Lavas with the higher abundance patterns are likely derived by fractional crystallization from magmas with the lower abundance patterns, including

plagioclase to produce the negative Sr anomalies. Axial High lavas generally have the steepest patterns, with the highest $La/Sm_N$ and high, but variable, $Tb/Yb_N$ (Figure 6; note that Yb abundances by INAA have been adjusted to better match ICP-MS data, see Section 3). Basalts from the adjacent Seminole Ridge are variable in incompatible element abundances and in the slope of the patterns, and have a range of both $La/Sm_N$ and $Tb/Yb_N$ ratios (Figure 6). SER South basalts also exhibit patterns with varying abundances and slopes, are generally less enriched in the most incompatible elements than Axial High lavas, and have $Tb/Yb_N$ between 1.05 and 1.28 (Figure 6). The 30´-Ridge basalts have uniform, flatter patterns than SER South lavas, but still have a peak in their patterns at Ta. Explorer Seamount basalts are all N-MORB, with pronounced depletion in the more incompatible elements compared to the less incompatible elements and near-flat middle to heavy REE slopes ($La/Sm_N < 1$, $Tb/Yb_N < 1.2$, Figure 6). It should be noted that some of the spread in rare earth element ratios may be due to differences in analytical techniques that include INAA, acid-dissolution ICP-MS, and laser-ablation ICP-MS. However, with the exception of Yb, the differences in rare earth element concentrations are small, and the conclusions drawn above are robust.

Incompatible element enrichment in the basalts follows a geographic pattern. High $K_2O/TiO_2$ basalts are mostly found around the Magic Mountain site and from two small cones on the east side of the Seminole Ridge, approximately 4 km east of Magic Mountain (RC-01, 02). These E-MORB lavas all have $La/Sm_N > 1.8$. Three rock cores (RC-03, -04, -05) sampled two small ridges midway between Magic Mountain and the RC-01 and -02 cones, and glasses from all three cores are T-MORB with lower $K_2O/TiO_2$ compositions. Michael et al. (1989) analyzed samples from three dredge/camera tows on the Seminole Ridge; all samples are T-MORB with $K_2O/TiO_2 < 0.21$, one has $Nb/Zr_N = 1.9$, and two others have $Nb/Zr_N \sim 1.45$. Most samples collected north and south of Magic Mountain are T- to N-MORB lavas with $La/Sm_N < 1.65$.

*4.2 Radiogenic Isotopes*

Explorer basalts have a wide range of isotopic compositions: $^{87}Sr/^{86}Sr = 0.70251$-$0.70297$, $^{143}Nd/^{144}Nd = 0.51319$-$0.51303$, $^{206}Pb/^{204}Pb = 18.827$-$19.261$, and $^{176}Hf/^{177}Hf = 0.28314$-$0.28301$ (Figure 7). There is a clear distinction between lavas from the northern

and southern regions of Explorer Ridge: Explorer Deep, North SER and lavas from the axial high region of the SER have the highest Sr and Pb, but lowest Nd and Hf isotope ratios. Sr, Nd and Pb isotope ratios correlate well with each other, but correlations between these isotopes and $^{176}Hf/^{177}Hf$ are more scattered (commonly some SER axial high samples are offset from the rest of the SER data array). There is also a good correlation between isotopic ratios and $La/Sm_N$ (Figure 8) and $K_2O/TiO_2$ vs. $La/Sm_N$ ($r^2$ = 0.92, not shown). Lavas with the greatest light-REE enrichment have the highest $^{87}Sr/^{86}Sr$ and Pb isotope ratios and the lowest $^{143}Nd/^{144}Nd$ (not shown) and $^{176}Hf/^{177}Hf$. Explorer Seamount basalts have the lowest $La/Sm_N$ in our sample suite and plot at the isotopically depleted end of the Explorer Ridge isotope ratio spectrum. Note that lavas from the Endeavour and West Valley segments of the northern Juan de Fuca ridge exhibit a range of $La/Sm_N$ that is close to that of Explorer basalts, but the range of isotopic compositions is lower.

Compared to previous isotopic work on Gorda/Juan de Fuca and northern East Pacific Rise basalts, Explorer Ridge lavas commonly have lower Nd and Hf isotope ratios, somewhat higher Sr ratios, and notably the most radiogenic Pb isotope ratios (Figures 9, 10) (e.g., Church and Tatsumoto, 1975; Davis et al., 2008; Salters et al., 2011; White et al., 1987). In particular, Hf isotopic ratios are generally low at a given Nd isotopic ratio in Explorer basalts compared to MORB from the Gorda Ridge and the northern East Pacific Rise, particularly in the most depleted lavas from SER South and Explorer Seamount (Salters et al., 2011). SER basalts also exhibit a wide range of isotopic ratios, far greater than the range for other northern Juan de Fuca ridge segments that host E-MORB such as the Endeavour and West Valley segments (Figures 8, 9, 10).

## 5. DISCUSSION

### *5.1 Within-Ridge Processes*

#### *5.1.1 Liquid Lines of Descent*

The composition of basalts erupted at mid-ocean ridges is strongly influenced by fractional crystallization and/or mixing between batches of parental melts in sub-axial magma chambers. Glassy basalts from the Axial High region of SER show evidence for

being related largely by fractional crystallization from similar, but not common, parental magmas. Ratios of incompatible elements such as $K_2O/Na_2O$, $K_2O/TiO_2$, La/Sm, and Ta/Hf are fairly uniform in SER basalts from the Axial High, and $CaO/Al_2O_3$, Ni, and Cr all decrease with decreasing Mg#. A simple major element oxide mass-balance calculation (Carr, 2012) suggests that removal of ~30% total solids from sample CR2-CV34 (Mg# = 0.63) in the proportions 5% olivine ($Fo_{75}$), 50% plagioclase ($An_{78}$), and 40% clinopyroxene produces a daughter composition similar to that of the most evolved axial high sample RC-06gl (Mg# = 0.51). The phase proportions are approximately those determined by least-squares modeling by Michael and Chase (1987) for SER basalts. Incompatible element abundances in the SER Axial High lavas generally increase by a factor of 1.7 to 1.8 from the least to most evolved magmas (high to low Mg#), also consistent with removal of ~30% solids from a parental magma. A key point is the importance of clinopyroxene fractionation in E-MORB from Explorer Ridge, likely due to high pressure crystallization and/or the relatively high $H_2O$ contents in primary basalts that suppresses plagioclase crystallization but enhances clinopyroxene crystallization (Michael and Chase, 1987).

Major element trends versus Mg# indicate as many as five liquid lines of descent (Figures 3, 4). The SER Axial High, SER North, and most SER Seminole glasses overlap in major element composition vs. Mg# ($CaO/Al_2O_3$, $K_2O$ shown in Figure 3), where clinopyroxene dominates the fractionation history. Basaltic glasses from Explorer Deep follow a different trend, with little change in $CaO/Al_2O_3$ and much less change in $K_2O$ with decreasing Mg#, and appear to be related by olivine +/- plagioclase crystallization. Explorer Seamount glasses are distinctive, with low $K_2O$ and $CaO/Al_2O_3$ (due to low CaO and high $Al_2O_3$ compared to SER lavas), high $FeO^t$, $Na_2O$ and $TiO_2$ (not shown). Explorer Seamount lavas exhibit little variation in composition compared to the SER segments. Most SER South glasses have low $K_2O$ at a given Mg# compared to the SER Axial High glasses, and form a negatively-sloping array below the SER Axial High glasses that partially overlaps the field for the West Valley segment. Finally, basalts from the 30´-Ridge (Jenner and O'Neill, 2012a) form arrays in Figure 3 with different slopes compared to all SER segments, and also have high $Na_2O$ (Figure 4) and $Al_2O_3$ contents (~16.5%) that approach the high $Al_2O_3$ of Explorer Seamount glasses (16.8-

17.8%). Experimental data indicate that the high $Na_2O$, $Al_2O_3$ but low CaO of Explorer Seamount and 30´-Ridge basalts are consistent with low degrees of melting of spinel peridotite (Fujii and Scarfe, 1985), but the high $Na_2O$ and $FeO^t$ are unusually high and suggest that some other component (pyroxenite??) in the upper mantle must be contributing to Explorer Seamount magmas.

At the same time, linear arrays in plots of isotope ratios versus trace element ratios are consistent with mixing of liquids (melts) along the length of the ridge (Figures 7, 8) (Langmuir et al., 1978; Michael et al., 1989). The abundances of two highly incompatible elements, such as Th and La, are highly correlated ($r^2 = 0.97$), whereas ratios of trace element with differing incompatibility (e.g., Th/La vs. Th/Yb, not shown) form curving arrays, all consistent with mixing of melts (Langmuir et al., 1978). The processes controlling the different liquid lines of descent do not appear to impact incompatible element and isotopic characteristics.

*5.1.2 Depth of Melting and Mantle Sources*

Explorer Ridge MORB require two mantle sources, one depleted and one enriched in terms of incompatible elements and radiogenic isotopes, that are also distinct in primitive mantle-normalized ratios of middle to heavy REE: $Tb/Yb_N$ range from 1.15 to 1.4 in E-MORB, from 1.05 to 1.3 in T-MORB, but are always < 1.18 in N-MORB (Figure 6). E-MORB from the Axial High have $Tb/Yb_N$ that are commonly greater than those of N-MORB from the East Pacific Rise (1.00 to 1.26, from Jenner and O'Neill, 2012a). The low $Tb/Yb_N$ of N-MORB is attributed to melting in the spinel peridotite stability field, and the higher ratios in E-MORB may reflect lower degrees of partial melting of spinel peridotite, the presence of a non-peridotite source lithology in the upper mantle, or melting in the garnet peridotite stability field (e.g., Arevalo and McDonough, 2010; Donnelly et al., 2004; Gill et al., 2016; van Westrenen et al., 2001; Waters et al., 2011). Starting from a spinel peridotite with rare earth concentrations typical of depleted upper mantle, the percentage of partial melt required to reproduce the trace element patterns of E-MORB is < 1% (e.g., Donnelly et al., 2004). This low degree of melting is not consistent with the robust magmatic nature of the Explorer Ridge axial high. Other E-

MORB studies conclude that the degree of partial melting for E- and N-MORB sources are approximately equal (Donnelly et al., 2004).

Melting of garnet peridotite would only occur in the deeper part of the melting column beneath the ridge, and low-degree melts of a garnet peridotite are too enriched in the light REE and too depleted in the heavy REE compared to most E-MORB (Figure 11, and Donnelly et al., 2004). However, the Explorer E-MORB could be produced by ~5% partial melting of a peridotite with 5% garnet, followed by crystal fractionation and a consequent increase in Yb concentration with little to no change in Ce/Yb. Yb concentrations increase, like other incompatible elements, as Mg# decreases in the SER Axial High E-MORB (Figure 3). However, the increase in Yb concentrations approaches 50% (in the ICP-MS data set alone), higher than the percent increase in most other incompatible elements, suggesting that fractional crystallization is not solely responsible for the observed Yb enrichment in the E-MORB. Regardless, these deep-derived melts must be able to migrate to the shallow subcrustal depths without interacting with shallow peridotites, or else the garnet signature would be diluted and the E-MORB samples would have more scattered Ce/Yb ratios. Lavas from south of the axial high could be considered to be mixtures of axial high E-MORB and ~10% melts of spinel peridotite, followed by fractional crystallization.

The enrichment in Nb over La in a potential garnet peridotite source for the Explorer E-MORB (and E-MORB from other localities, e.g., Donnelly et al., 2004; Waters et al., 2011) requires some explanation, since Nb and La are fractionated only at low degrees of partial melting, <1% (e.g., Donnelly et al., 2004). As modeled here, at higher degrees of melting the small bulk $K_D$ difference between Nb and La in a typical peridotite will produce a melt with only a small or no positive Nb anomaly. Thus, the garnet peridotite must be enriched in Nb and Ta by some process prior to melting beneath the ridge. Also, the garnet peridotite was enriched in incompatible elements over a long timeframe, such that melts from the garnet peridotite have higher Sr, Pb and lower Nd isotope ratios than melts from the spinel peridotite with a DM composition. A Primitive Mantle-like source would contribute to the higher Sr and lower Nd isotopic ratios characteristics of Explorer Ridge E-MORB, although Pb and Hf isotope ratios are not consistent with a possible mixing trend between DM and Primitive Mantle.

Several studies of E-MORB have concluded that garnet pyroxenite is a minor but chemically influential lithology in the upper mantle (e.g., Arevalo and McDonough, 2010; Gill et al., 2016; Hirschmann, 1994; Lambart et al., 2009; Pertermann and Hirschmann, 2003). Garnet is stable to shallower mantle depth in a pyroxenite lithology, and pyroxenite can melt to much higher degrees than peridotite beneath a mid-ocean ridge. An "old" (e.g., recycled basaltic crust) pyroxenite lithology embedded in an upper mantle peridotite would also be different isotopically from the peridotite, and would likely produce melts with enriched trace element characteristics and higher Sr and Pb isotopic ratios. Higher degrees of melting of pyroxenite beneath the ridge axis would also lead to thicker crust and shallower water depth above the ridge. The anomalously shallow depth of the Explorer Ridge axial high implicates a high melt contribution from pyroxenite, and the decrease in incompatible element enrichment with increasing water depth to the south is consistent with a lesser melt contribution from pyroxenite (as inferred for the shallow "inflated" versus deeper "graben" stages at the Endeavour Segment by Gill et al., 2016). Figure 11 includes partial melting curves for a model garnet pyroxenite (see caption for model details). Pyroxenite partial melts have considerably higher Yb concentrations than measured in Explorer E-MORB, due primarily to the higher Yb concentration in the pyroxenite starting composition (grey star). Explaining the most Mg-rich and Yb-poor E-MORB at Explorer Ridge would require mixing of ~20% partial melt of a garnet pyroxenite with ~4% melt of a garnet peridotite in the proportions 15/85, followed by fractional crystallization. T-MORB and N-MORB require progressively lesser contributions from garnet-bearing lithologies and approach the spinel peridotite melting curve. Trace element modeling supports a garnet-bearing source for Explorer Ridge E-MORB, but is equivocal concerning a peridotite or pyroxenite lithology. Unfortunately, experimental determination of the major element compositions of high percentage melts of garnet pyroxenite and lower-percent melts of peridotite show that the two melt types are very similar (both are basaltic), and thus major elements are generally not useful in distinguishing pyroxenite-derived melts at mid-ocean ridges (Lambart et al., 2009).

Gill et al. (2016) suggest that magmas erupted during periods of more robust volcanism at the Endeavour Segment (Inflated Ridge Trend) tap a mixed peridotite-

pyroxenite source, whereas eruptions during periods of more muted volcanism (Graben Trend) require a mixed peridotite source with only a minor pyroxenite contribution. We note that the robust volcanism at the Axial High region on Explorer Ridge is perhaps the best evidence for a pyroxenite lithology as the source of E-MORB, along with the incompatible element and isotopic characteristics of Axial High basalts. A single seismic refraction line across the SER, crossing the ridge just south of the Axial High, indicates that crustal thickness is high, between 8 and 10 km, compared to a typical East Pacific Rise crustal thickness of 6-7 km (Malecek and Clowes, 1978). This excess crustal thickness could be due to excess magmatism, but could also result from crustal deformation on the southeast side of SER (Riddihough, 1977).

*5.2 Isotopic Components in the Northeast Pacific Upper Mantle*

Previous geochemical studies of basalts from the Explorer Ridge have documented the presence of both E-type and N-type MORB along the ridge (Cousens, 2010; Cousens et al., 1984; Michael et al., 1989). Studies of the spreading centres north of the Cobb Offset have shown that E-MORB are also common along the northern Juan de Fuca Ridge (Allan et al., 1993; Cousens et al., 1995; Gill et al., 2016; Karsten et al., 1990; Kelley et al., 2012; Woodcock et al., 2006; Woodcock et al., 2007). The Juan de Fuca system north of the Cobb Offset is a distinct E-MORB province in the Pacific Ocean (Figure 2). In addition, basalts with enriched trace element patterns and more intraplate isotopic compositions have been analyzed from the Pratt-Welker, Cobb-Eickelberg and other intraplate seamounts in the northeast Pacific Ocean (Chadwick et al., 2014; Cousens, 1988; Cousens et al., 1985; Desonie and Duncan, 1990; Dreyer et al., 2013; Hegner and Tatsumoto, 1989; Keller et al., 1997; Rhodes et al., 1990). Until now, few published isotopic data existed for the Explorer Ridge (Michael et al., 1994), and our new data, especially with the increased precision of modern analytical techniques, allow us to evaluate the origin of the isotopically enriched component(s) in northeast Pacific E-MORB.

Figure 9 presents isotopic data for the East Pacific Rise, Explorer, Juan de Fuca and Gorda ridges, as well as data from the Cobb-Eickelberg-Axial seamount track and the Tuzo Wilson volcanic field, to evaluate trends towards mantle endmembers identified

from studies of ocean island basalts. Hf isotopic data are only available for the Cobb-Eickelberg seamounts, Gorda Ridge, Endeavour Segment and Explorer Ridge basalts. The Explorer, northern Juan de Fuca Ridge, and Endeavour basalts form overlapping arrays in a plot of $^{87}Sr/^{86}Sr$ vs. $^{143}Nd/^{144}Nd$, $^{87}Sr/^{86}Sr$ vs. $^{206}Pb/^{204}Pb$, and $^{207}Pb/^{204}Pb$ vs. $^{206}Pb/^{204}Pb$ plots (Figure 9A, B, D) that trend between DMM and a composition intermediate between HIMU and FOZO. The trend appears to be linear, implying roughly similar Sr/Nd and Sr/Pb in the depleted and enriched mantle endmembers for Explorer and northern Juan de Fuca Ridge basalts. In contrast, Gorda Ridge MORB are commonly displaced to higher $^{87}Sr/^{86}Sr$, relative to Explorer Ridge basalts, at a given $^{143}Nd/^{144}Nd$ (Figure 9A). The same is true of many Tuzo Wilson volcanic field lavas, possibly due to incorporation of Sr from seawater.

In a $^{207}Pb/^{204}Pb$ vs. $^{206}Pb/^{204}Pb$ plot (Figure 9D), the Explorer Ridge data array plots just below the Northern Hemisphere Reference Line (NHRL, Hart, 1984). Although there is some scatter in the Pb data (TIMS analyses), the northern Juan de Fuca Ridge basalts overlap with the array of the Explorer basalts. In contrast, the Gorda Ridge MORB follow a much steeper trend, suggesting that they include an EM component that is not observed in Explorer and northern Juan de Fuca MORB (Figure 9B). Tuzo Wilson volcanic field lavas straddle the Explorer Ridge Pb isotope array (Allan et al., 1993; Cousens, 1988).

In Nd-Hf isotopic space (Figure 7C), the Explorer Ridge basalts have remarkably low $^{176}Hf/^{177}Hf$ at their $^{143}Nd/^{144}Nd$ compared to any other mid-ocean ridge segment studied to date. They plot roughly on a trend between a depleted endmember with a lower εHf (and hence lower Lu/Hf than typical Pacific depleted upper mantle) than the Gorda Ridge, East Pacific Rise and Endeavour segment basalts and an enriched endmember between FOZO and HIMU, the latter being the only mantle component that has demonstrably low $^{176}Hf/^{177}Hf$ at a given $^{143}Nd/^{144}Nd$ amongst ocean island basalts (e.g., Salters et al., 2011; Stracke et al., 2005). The result is an Explorer Ridge data array with a much lower slope than the Terrestrial Array. In a plot of $^{176}Hf/^{177}Hf$ vs. $^{208}Pb^*/^{206}Pb^*$ (Stracke et al., 2005), the low $^{176}Hf/^{177}Hf$ and $^{208}Pb^*/^{206}Pb^*$ (0.912 – 0.899) of the Explorer Ridge basalts are almost unique amongst MORB, and the basalts plot between the Endeavour segment MORB and HIMU-type ocean island basalts (Figure 10; e.g.,

Raivavae, Tubuai). In summary, the isotopic characteristics of Northeast Pacific seafloor basalts are neither uniform nor easily explained, and results to date suggest that this area should be a high priority for future geochemical investigations.

*5.3 Distribution of the Enriched Component Beneath the NE Pacific*

The various volcanic features in the NE Pacific appear to share a near-common depleted mantle component, with low Sr, Hf and Pb isotope ratios and high Nd isotope ratios. The depleted component is exemplified in the majority of northern Juan de Fuca Ridge basalts (including the Endeavour depleted basalts), with the exception of the low Hf isotope ratios that are unique to the Explorer ridge. Such a depleted mantle component is also shared by "depleted" MORB from the northern East Pacific Rise. Lavas from the Gorda Ridge commonly have the lowest Sr and Pb, or highest Nd and Hf, isotope ratios in Northeast Pacific MORB. In the case of the Explorer Ridge, the most "depleted" rocks are from the Explorer Seamount, but these lavas also do not reach the extreme depleted isotopic values exhibited by Gorda Ridge basalts. The same is true of highly depleted lavas from the Heck and Heckle seamounts on the west flank of the West Valley segment of the northern Juan de Fuca Ridge (Cousens et al., 1995).

Unlike the case for a common depleted mantle component, the different volcanic features shown in Figure 9 appear to require different enriched components. The Sr-Nd isotopic array for the Explorer Ridge basalts suggests an enriched component with a composition between that of FOZO and HIMU. MORB from the Endeavour and West Valley segments of the Juan de Fuca ridge also follow the isotopic trends shown by Explorer basalts in Figure 9 but do not approach the extreme La/Sm and isotopic ratios of some Explorer E-MORB.

Lavas from the northwestern Cobb-Eickelberg seamount chain have the highest Pb and lowest Hf isotopic ratios of all seafloor rocks in the NE Pacific Ocean (Chadwick et al., 2014), and both the Cobb-Eickelberg intraplate lavas and Explorer Ridge E-MORB lava suites trend towards a similar enriched endmember with a HIMU or FOZO composition. The Cobb-Eickelberg studies indicate that the HIMU or FOZO component has been distributed in the NE Pacific upper mantle for at least the past ~30 Ma (oldest

lava ages in the northwest Cobb-Eickelberg chain, Dalrymple et al., 1987; Keller et al., 1997).

At Explorer Ridge, E-MORB are most abundant at the axial high, leading to a previous proposal that the axial high is underlain by a mini-plume or hotspot (Michael et al., 1989). The high Ta/La and Ta/Th of Explorer Ridge E-MORB (note Nb and Ta are coupled) is also common in many ocean island basalts (Willbold and Stracke, 2006), and thus enriched components in E-MORB are commonly thought to be similar in origin to those in intraplate basalts (e.g., Niu et al., 2002). One interpretation to account for the geochemical gradient from abundant E-MORB, with intraplate-like trace element character, erupted in the axial high area to more N-MORB-like compositions to the south (this study) and to the north (Northern Explorer Rifts segments, Figure 1A, see Cousens et al., 1984; Michael et al., 1989) is that either mantle or melts from a hotspot mingle or mix with either mantle or melts of depleted upper mantle to a greater extent going both south and north from the hotspot center.

However, in contrast to other regions of plume-ridge interaction (e.g., Fontignie and Schilling, 1996; Schilling, 1991; White et al., 1986), including Axial Seamount on the southern Juan de Fuca Ridge that marks the current location of the Cobb-Eickelberg hotspot (Chadwick et al., 2005; Karsten and Delaney, 1989), there is no seamount edifice on or adjacent to SER that would clearly indicate the presence of a hotspot. The same is true of other E-MORB localities along the northern Juan de Fuca ridge system (Cousens et al., 1995; Gill et al., 2016). We therefore conclude that a mini-plume model for the origin of E-MORB at Explorer is not required.

## 6. CONCLUSIONS

Basalt lavas collected from the length of the Southern Explorer Ridge exhibit a wide range of major element, trace element and isotopic compositions consistent with mixing of melts from a depleted mantle (DM) and enriched mantle components. The shallowest section of the ridge, the axial high, erupts E-MORB lavas with the greatest contribution from the enriched mantle source, but also includes some lavas with a DM contribution.

Basalts collected to the south of the axial high become progressively more DM-like in trace element and isotopic composition, and basalts from the south end of the ridge are N-MORB. High Pb and low Hf isotopic ratios indicate that the enriched mantle component has a FOZO to HIMU composition that is also observed in E-MORB from the northern Juan de Fuca Ridge (West Valley, Endeavour segments) but not in Juan de Fuca Ridge basalts south of the Endeavour segment or in Gorda Ridge basalts. Thus, the Cobb Offset is currently a boundary between a mixed DM-FOZO or DM-HIMU mantle to the north and a predominantly DM mantle to the south. The isotopic and trace element data are consistent with previous proposals that the FOZO or HIMU component is locally distributed beneath the Explorer and northern Juan de Fuca ridges but is not associated with an underlying hotspot.

## 6. ACKNOWLEDGEMENTS

We appreciate technical assistance in the isotope laboratories at the IGGRC, Carleton University and the PCIGR at UBC. We thank R.L. Chase for making the pre-1993 UBC collection available for sampling. BLC thanks Bob Embley for the opportunity to participate in the 2002 NOAA Ocean Exploration cruise to Explorer Ridge, and Kathy Gillis, Cathy Channing, Anthony Williams-Jones, Bill Chadwick and the RV T.G. Thompson and ROV ROPOS crew for support during the cruise. Bob Embley kindly shared the map of the Explorer Ridge area (Figures 1A, 1B). Dan Fornari and Mike Perfit provided the rock corer, wax, and other materials for the rock coring program. M. Constantin was supported by an NSERC postdoctoral fellowship. Funding for UBC/UT research cruises was from NSERC Operating and NSERC Shiptime grants to Scott and R.L. Chase. The 2002 NOAA cruise was funded through the NOAA Ocean Exploration program and a NSERC CRD grant to A.E. Williams-Jones. Analytical costs were funded through Scotiabank research grants to Scott, a NSERC Collaborative Special Projects grant to Scott, Constantin, Cousens and M. Gorton, and NSERC Operating/Discovery grants to Scott, Weis and Cousens. We thank Editors Andreas Stracke and Marc Norman and the journal reviewers for their comments and suggestions for improvement of the manuscript. This is IGGRC Contribution Number 60.

Extra References from data tables: (Jochum et al., 2016) (Stix and Gorton, 1992) (Jarosewich et al., 1980)

FIGURE CAPTIONS

Figure 1A. Geological map of the Explorer Ridge area showing major tectonic features. (modified after a map provided by R.W. Embley). Contour intervals are 500 m. DK = Dellwood Knolls. DS = Dellwood Seamounts. ED: Explorer Deep. ES = Explorer Seamount. ET = Explorer Trough. MM (cross) = Magic Mountain hydrothermal field. NER: Northern Explorer Rifts. PRR = Paul Revere Ridge. RDFZ = Revere-Dellwood Fracture Zone. SER = Southern Explorer Ridge. SFZ = Sovanco Fracture Zone. SR = Seminole Ridge segment. SS = Seminole Seamount. TWVF = Tuzo Wilson Volcanic Field. WB = Winona Basin. WR = Winona Ridge. Area of Figure 1B is indicated by dashed box. Inset: Subdivisions of the Juan de Fuca plate system. Axial = Axial Seamount.

Figure 1B. Locations of samples analyzed in this study. Abbreviations as in Figure 1A. "MM" = Magic Mountain hydrothermal field. "J&O'N 2012" = sample locations of glass analyses in Jenner and O'Neill (2012) that are included in the following figures. "Smt" = Seamount.

Figure 2. Variation in $La/Sm_N$ (N = Primitive mantle-normalized, values from Sun and McDonough, 1989) vs. latitude (degrees North) along the Juan de Fuca / Explorer Ridge system. Axial = Axial Seamount. Dellwood = Dellwood Knolls. SJdF = Southern Juan de Fuca Ridge. Seg = Segment. TWVF = Tuzo Wilson Volcanic Field. (Data from Allan et al., 1993; Cousens et al., 1995; Cousens et al., 1984; Karsten et al., 1990; Michael et al., 1989; Rhodes et al., 1990; Smith et al., 1994; Stakes and Franklin, 1994; Van Wagoner and Leybourne, 1991).

Figure 3. Variations in major element and trace element chemistry with $Mg/(Mg+Fe^{2+})$ in Explorer Ridge basalts. $Fe^{2+} = 0.9*Fe^{total}$. Fields for Endeavour Segment, West Valley Segment, and Southwest Seamount (SWS, south end of West Valley) from Gill et al. (2016) and Cousens et al. (1995).

Figure 4. $FeO^t$ and $Na_2O$ vs. MgO in Explorer Ridge lavas of this study and Jenner and O'Neill (2012a). Dashed lines are best-fit lines through Axial High samples.

Figure 5. Primitive mantle-normalized incompatible element patterns for some Explorer Ridge basalts. A. Explorer Deep and SER North. B. Axial High glasses (grey) and whole-rock (black) analyses. C. Seminole Ridge and 30´-Ridge glasses. D. SER South and Explorer Seamount. Normalizing factors are from Sun and McDonough (1989). Note scale change for Panel D.

Figure 6. Primitive mantle-normalized $La/Sm_N$ vs. $Tb/Yb_N$ in Explorer Ridge basalts. Small grey crosses enclosed in dashed field are Endeavour Segment lavas (Gill et al., 2016). Dotted field encloses northern and southern East Pacific Rise basalts (Jenner and O'Neill, 2012a). Normalizing factors are from Sun and McDonough (1989). Explorer Ridge samples with Yb determined by INAA have Yb concentrations adjusted to be more consistent with ICP-MS Yb determinations according to the formula in Section 3.

Figure 7. Isotopic data for Explorer Ridge basalts. Two-sigma error bars and ellipses are shown. Multicollector ICP-MS Pb analyses have analytical errors smaller than the data symbols, but TIMS Pb analyses have the errors shown in the figure. Arrows show the south to north variation in isotopic compositions.

Figure 8. Isotope ratios vs. $La/Sm_N$ in Explorer basalts (N = Primitive mantle-normalized, values from Sun and McDonough, 1989). Endeavour (dashed field) and West Valley (dot-dash field) segment sources as in Figure 3.

Figure 9. Sr, Nd, Pb and Hf isotope ratios in northern East Pacific Rise (EPR), Gorda Ridge, Juan de Fuca Ridge (N = north of Cobb Offset, S = south of Cobb Offset), Endeavour Segment, Cobb-Eickelberg seamounts, and the Tuzo Wilson volcanic field compared to Explorer basalts of this study. NHRL = Northern Hemisphere Reference Line (Hart, 1984). Mantle endmembers (from Stracke et al., 2005): DMM = depleted MORB mantle, HIMU = high-μ, FOZO = Focal Zone, EM = Enriched Mantle (I and II). Endeavour Segment lavas from Gill et al. (2016). Data from Church and Tatsumoto, 1975; Cousens et al., 1995; Davis et al., 2008; Davis et al., 1998; Hegner and Tatsumoto, 1987; PetDB, 2015; Salters et al., 2011; White et al., 1987).

Figure 10: $^{176}Hf/^{177}Hf$ vs. $^{208}Pb^*/^{206}Pb^*$ (as defined by Abouchami et al., 2005) comparing northern East Pacific Rise (EPR) and Gorda Ridge (PetDB, 2015), Endeavour Segment (Gill et al., 2016), and Cobb-Eickelberg-Axial seamount basalts (Chadwick et al., 2014) to Explorer Ridge lavas (filled triangles), non-HIMU type ocean island basalts (OIB), HIMU-type OIB, and the estimated composition of FOZO (figure modified from Stracke et al., 2005).

Figure 11. Ce/Yb vs. Yb concentration (ppm) showing non-modal, batch partial melting models (Shaw, 1970) for spinel peridotite, garnet peridotite, and garnet pyroxenite ("GP", grey lines and symbols; stars = bulk compositions). Explorer samples with Yb determined by INAA have Yb concentrations adjusted to be more consistent with ICP-MS Yb determinations according to the formula in Section 3. Fractional crystallization drives residual liquids to the right. Numbers beside black and grey symbols indicate percent partial melting. For peridotite models, starting compositions assume DM concentrations, modal abundances, and D values from Salters and Stracke (2004). For the garnet pyroxenite model, the starting composition is N-MORB (Sun and McDonough, 1989) with the phase proportions ol:opx:cpx:gar = 0.1:0.25:0.55:0.10 and D values from Pertermann et al. (2004). Black curve with tick marks indicates mixtures of 4% melt of garnet peridotite with 20% melt of garnet pyroxenite, with each tick mark indicating a 25% increment in the mix.

**REFERENCES**

Abouchami, W., Hofmann, A.W., Galer, S.J.G., Frey, F.A., Eisele, J. and Feigenson, M. (2005) Lead isotopes reveal bilateral asymmetery and vertical continuity in the Hawaiian mantle plume. *Nature* **434**, 851-856.

Allan, J.F., Chase, R.L., Cousens, B.L., Michael, P.J., Gorton, M.P. and Scott, S.D. (1993) The Tuzo Wilson volcanic field, NE Pacific: alkaline volcanism at a complex, diffuse, transform-trench-ridge triple junction. *J. Geophys. Res.* **98**, 22367-22387.

Andres, M., Blichert-Toft, J. and Schilling, J. (2004) Nature of the depleted upper mantle beneath the Atlantic: evidence from Hf isotopes in normal mid-ocean ridge basalts from 79oN to 55oS. *Earth Planet. Sci. Lett.* **225**, 89-103.

Arevalo, R., Jr. and McDonough, W.F. (2010) Chemical variations and regional diversity observed in MORB. *Chem. Geol.* **271**, 70-85, doi: 10.1016/j.chemgeo.2009.12.013.

Atwater, T. (1970) Implications of plate tectonics for the Cenozoic tectonic evolution of western North America. *Geol. Soc. Amer. Bull.* **81**, 3513-3536.

Atwater, T. and Stock, J. (1998) Pacific-North America plate tectonics of the Neogene Southwestern United States: An update, in: Ernst, W.G., Nelson, C.A. (Eds.), *Integrated Earth and Environmental Evolution of the Southwestern United States*. Bellweather (Geological Society of America), Columbia, MD., pp. 393-420.

Bertrand, W.G. (1972) A geological reconnaissance of the Dellwood Seamount area, northeast Pacific Ocean, and its relationship to plate tectonics. University of British Columbia, Vancouver, p. 151.

Bjerkgard, T., Cousens, B.L. and Franklin, J.M. (2000) Metal sources for the Middle Valley sulphide deposits, northern Juan de Fuca Ridge. *Econ. Geol.* **95**, 1473-1488.

Botros, M. and Johnson, H.P. (1988) Tectonic evolution of the Explorer-Northern Juan de Fuca region from 8 Ma to the present. *J. Geophys. Res.* **93**, 10421-10438.

Carbotte, S.M., Dixon, J.M., Farrar, E., Davis, E.E. and Riddihough, R.P. (1989) Geological and geophysical characteristics of the Tuzo Wilson Seamounts: implications for plate geometry in the vicinity of the Pacific-North America-Explorer triple junction. *Can. J. Earth Sci.* **26**, 2365-2384.

Caress, D.W., Menard, H.W. and Hey, R.N. (1988) Eocene reorganization of the Pacific-Farallon spreading center north of the Mendocino Fracture Zone. *J. Geophys. Res.* **93**, 2813-2838.

Carr, M. (2012) Igpet for Mac, 16 May 2012 ed. Terra Softa Inc.

Chadwick, J., Keller, R.A., Kamenov, G., Yogodzinski, G.M. and Lupton, J.E. (2014) The Cobb hot spot: HIMU-DMM mixing and melting controlled by a progressively thinning lithospheric lid. *Geochem. Geophys. Geosyst.* **15**, 3107-3122, doi: 10.1002/2014GC005334.

Chadwick, J., Perfit, M.R., Ridley, I., Jonasson, I., Kamenov, G., Chadwick, W.W., Embley, R.W., le Roux, P. and Smith, M. (2005) Magmatic effects of the Cobb hotspot on the Juan de Fuca Ridge. *J. Geophys. Res.* **110**, B03101.

Chase, R.L., Johnson, H.P. and Ryall, P.J.C. (1982) Geology of Explorer Seamount, NE Pacific. *EOS, Trans. Amer. Geophys. Union* **63**, 1154.

Church, S.E. and Tatsumoto, M. (1975) Lead isotope relations in ocean ridge basalts from the Juan de Fuca-Gorda Ridge area, N.E. Pacific Ocean. *Contributions to Mineralogy Petrology* **53**, 253-279.

Cousens, B.L. (1988) Isotopically depleted, alkalic lavas from Bowie Seamount, northeast Pacific Ocean. *Can. J. Earth Sci.* **25**, 1708-1716.

Cousens, B.L. (1996) Magmatic evolution of Quaternary mafic magmas at Long Valley Caldera and the Devils Postpile, California: Effects of crustal contamination on lithospheric mantle-derived magmas. *J. Geophys. Res.* **101**, 27673-27689.

Cousens, B.L. (2010) The geology and petrology of seafloor volcanic rocks of the northeastern Pacific Ocean, Offshore Canada. *Geoscience Canada* **37**, 49-64.

Cousens, B.L., Allan, J.F., Leybourne, M.I., Chase, R.L. and Van Wagoner, N. (1995) Mixing of magmas from enriched and depleted mantle sources in the northeast Pacific: West Valley segment, Juan de Fuca Ridge. *Contrib. Mineral. Petrol.* **120**, 337-357.

Cousens, B.L., Chase, R.L. and Schilling, J.-G. (1984) Basalt geochemistry of the Explorer Ridge area, northeast Pacific. *Can. J. Earth Sci.* **21**, 157-170.

Cousens, B.L., Chase, R.L. and Schilling, J.-G. (1985) Geochemistry and origin of volcanic rocks from Tuzo Wilson and Bowie Seamounts, northeast Pacific Ocean. *Can. J. Earth Sci.* **22**, 1609-1617.

Dalrymple, G.B., Clague, D.A., Vallier, T.L. and Menard, H.W. (1987) $^{40}Ar/^{39}Ar$ age, petrology, and tectonic significance of some seamounts in the Gulf of Alaska, in: Keating, B.H., Fryer, P., Batiza, R., Boehlert, G.W. (Eds.), Seamounts, Islands, and Atolls. American Geophysical Union, Geophysical Monograph 43, Washington, D.C., pp. 297-318.

Davis, A.S., Clague, D.A., Cousens, B.L., Keaten, R. and Paduan, J.B. (2008) Geochemistry of basalt from the North Gorda segment of the Gorda Ridge: Evolution toward ultraslow spreading ridge lavas due to decreasing magma supply. *Geochem. Geophys. Geosyst.* **9**, doi: 10.1029/2007GC001775.

Davis, A.S., Clague, D.A. and White, W.M. (1998) Geochemistry of basalt from Escanaba Trough: Evidence for sediment contamination? *J. Petrol.* **39**, 841-858.

Davis, E.E. and Currie, R.G. (1993) Geophysical observations of the northern Juan de Fuca Ridge system: lessons in sea-floor spreading. *Can. J. Earth Sci.* **30**, 278-300.

Desonie, D.L. and Duncan, R.A. (1990) The Cobb-Eickelberg Seamount Chain: hotspot volcanism with MORB affinity. *J. Geophys. Res.* **95**, 12697-12712.

Dixon, J.E., Clague, D.A. and Eissen, J.-P. (1986) Gabbroic xenoliths and host ferrobasalt from the southern Juan de Fuca Ridge. *J. Geophys. Res.* **91**, 3795-3820.

Donnelly, K.E., Goldstein, S.L., Langmuir, C.H. and Spiegelman, M. (2004) Origin of enriched ocean ridge basalts and implications for mantle dynamics. *Earth Planet. Sci. Lett.* **226**, 347-366, doi: 10.1016/j.epsl.2004.07.019.

Dreyer, B., Clague, D.A. and Gill, J.B. (2013) Petrological variability of recent magmatism at Axial seamount summit, Juan de Fuca ridge. *Geochem. Geophys. Geosyst.* **14**, 4306-4333, doi: 10.1002/ggge.20239.

Dziak, R.P. (2006) Explorer deformation zone: Evidence of a large shear zone and reorganization of the Pacific-Juan de Fuca-North America triple junction. *Geology* **34**, 213-216.

Eaby, J., Clague, D. and Delaney, J. (1984) Sr isotopic variations along the Juan de Fuca Ridge. *J. Geophys. Res.* **89**, 7883-7890.

Embley, R.W. (2002) Rediscovery and exploration of Magic Mountain, Explorer Ridge. *EOS, Trans. Amer. Geophys. Union,* **83** (47) Fall Meeting Supplement, Abs. T11C-1264.

Fontignie, D. and Schilling, J.-G. (1996) Mantle heterogeneities beneath the South Atlantic: A Nd-Sr-Pb isotope study along the Mid-Atlantic Ridge (3°S-46°S). *Earth Planet. Sci. Lett.* **142**, 209-221.

Fujii, T. and Scarfe, C.M. (1985) Composition of liquids coexisting with spinel lherzolite at 10 kbar and the genesis of MORBs. *Contrib. Mineral. Petrol.* **90**, 18-28.

Galer, S.J.G. and Abouchami, W. (1998) Practical application of lead triple spiking for correction of instrumental mass discrimination. *Mineralogical Magazine* **62A**, 491-492 (abs).

Gill, J., Michael, P., Woodcock, J.P., Dreyer, B., Ramos, F., Clague, D.A., Kela, J., Scott, S., Konrad, K. and Stakes, D.S. (2016) Spatial and temporal scale of mantle enrichment at the Endeavour Segment, Juan de Fuca Ridge. *J. Petrol.* **57**, 863-896.

Hart, S.R. (1984) A large scale isotope anomaly in the Southern Hemisphere mantle. *Nature* **309**, 753-757.

Hegner, E. and Tatsumoto, M. (1987) Pb, Sr, and Nd isotopes in basalts and sulphides from the Juan de Fuca Ridge. *J. Geophys. Res.* **92**, 11380-11385.

Hegner, E. and Tatsumoto, M. (1989) Pb, Sr, and Nd isotopes in seamount basalts from the Juan de Fuca Ridge and Kodiak-Bowie Seamount Chain, northeast Pacific. *J. Geophys. Res.* **94**, 17839-17846.

Hirschmann, M.M. (1994) Can garnet signature in MORB be derived from garnet pyroxenite in MORB source regions?, Geological Society of America Annual Meeting, Abstracts with Program **26**, p. A38.

Hoernle, K., Hauff, F., Kokfelt, T.F., Haase, K.M., Garbe-Schonberg, D. and Werner, R. (2011) On- and off-axis chemical heterogeneities along the South Atlantic Mid-Ocean-Ridge (5–11°S): Shallow or deep recycling of ocean crust and/or intraplate volcanism? *Earth Planet. Sci. Lett.* **306**, 86-97.

Jarosewich, E., Nelen, J.A. and Norberg, J.A. (1980) Reference samples for electron microprobe analysis. *Geostand. Newsletter* **4**, 43-47.

Jenner, F.E. and O'Neill, H.S.C. (2012a) Analysis of 60 elements in 616 ocean floor basaltic glasses. *Geochem. Geophys. Geosyst.* **13**, Q02005, doi: 10.1029//2011GC004009.

Jenner, F.E. and O'Neill, H.S.C. (2012b) Major and trace analysis of basaltic glasses by laser-ablation ICP-MS. *Geochem. Geophys. Geosyst.* **13**, Q03003, doi: 10.1029//2011GC003890.

Jochum, K.P., Weis, U., Schwager, B., Stoll, B., Wilson, S.A., Haug, G.H., Andreae, M.O. and Enzweiler, J. (2016) Reference Values Following ISO Guidelines for Frequently Requested Rock Reference Materials. *Geostandards Newsletter* **40**, 333-350.

Kappel, E.S. and Ryan, W.B.F. (1986) Volcanic episodicity and a non-steady state rift valley along northeast Pacific spreading centers: evidence from Sea MARC I. *J. Geophys. Res.* **91**, 13925-13940.

Karsten, J.L. and Delaney, J.R. (1989) Hot spot-ridge crest convergence in the northeast Pacific. *J. Geophys. Res.* **94**, 700-712.

Karsten, J.L., Delaney, J.R., Rhodes, J.M. and Liias, R.A. (1990) Spatial and temporal evolution of magmatic systems beneath the Endeavour Segment, Juan de Fuca Ridge: tectonic and petrologic constraints. *J. Geophys. Res.* **95**, 19235-19256.

Keller, R.A., Fisk, M.R., Duncan, R.A. and White, W.M. (1997) 16 m.y. of hotspot and nonhotspot volcanism on the Patton-Murray seamount platform, Gulf of Alaska. *Geology* **25**, 511-514.

Kelley, D.S., Carbotte, S.M., Caress, D.W., Clague, D.A., Delaney, J.R., Gill, J., Hadaway, H., Holden, J.F., Hooft, E.E.E., Kellogg, J.P., Lilley, M.D., Stoermer, M., Toomey, D.R., Weekly, R. and Wilcock, W.S.D. (2012) Endeavour Segment of the Juan de Fuca Ridge. *Oceanography* **25**, 44-61.

Klein, E.M. and Langmuir, C.H. (1987) Global correlations of ocean ridge basalt chemistry with axial depth and crustal thickness. *J. Geophys. Res.* **92**, 8089-8115.

Klein, E.M. and Langmuir, C.H. (1989) Local vs. global variations in ocean ridge basalt composition: a reply. *J. Geophys. Res.* **94**, 4241-4252.

Lambart, S., Laporte, D. and Schiano, P. (2009) An experimental study of pyroxenite partial melts at 1 and 1.5 GPa: Implications for the major-element composition of Mid-Ocean Ridge Basalts. *Earth Planet. Sci. Lett.* **288**, 335-347.10.1016/j.epsl.2009.09.038.

Langmuir, C.H., Vocke Jr., R.D. and Hanson, G., N, (1978) A general mixing equation with applications to Icelandic basalts. *Earth Planet. Sci. Lett.* **37**, 380-392.

Le Roex, A.P., Dick, H.J.B. and Watkins, R.T. (1992) Petrogenesis of anomalous K-enriched MORB from the Southwest Indian Ridge: 11°53'E to 14°38'E. *Contrib. Mineral. Petrol.* **110**, 253-268.

Lupton, J.E., Graham, D.W., Delaney, J.R. and Johnson, H.P. (1993) Helium isotope variations in Juan de Fuca Ridge basalts. *Geophys. Res. Lett.* **20**, 1851-1854.

Macdougall, J.D. and Lugmair, G.W. (1985) Extreme isotopic homogeneity among basalts from the southern East Pacific Rise: mantle or mixing effect? *Nature* **313**, 209-211.

Malecek, S.J. and Clowes, R.M. (1978) Crustal structure near Explorer Ridge from a marine deep seismic sounding survey. *J. Geophys. Res.* **83**, 5899-5912.

Menard, H.W. (1978) Fragmentation of the Farallon Plate by pivoting subduction. *J. Geol.* **86**, 99-10.

Michael, P.J. and Chase, R.L. (1987) The influence of primary magma composition, H2O, and pressure on mid-ocean ridge basalt differentiation. *Contrib. Mineral. Petrol.* **96**, 245-263.

Michael, P.J., Chase, R.L. and Allan, J.F. (1989) Petrologic and geologic variations along the South Explorer Ridge, northeast Pacific Ocean. *J. Geophys. Res.* **94**, 13895-13918.

Michael, P.J., Chase, R.L. and Armstrong, R.L. (1994) A combined Pb-Nd-Sr isotopic and trace element study of mid-ocean ridge basalts from Explorer Ridge, northeast Pacific, in: Lanphere, M.A., Dalrymple, G.B., Turrin, B.D. (Eds.), ICOG 8 abstracts, US Geological Survey Circular 1107, p. 217.

Mingxian, W., Ryall, P.J.C. and Bryan, J. (1986) A magnetic survey of Explorer Seamount - Recent spreading at the Explorer Trench. *Chin. J. Oceanol. Limnol.* **4**, 183-195.

National Oceanic and Atmospheric Administration (2002a) Ocean Explorer Explorations: Submarine Ring of Fire. URL: http://oceanexplorer.noaa.gov/explorations/02fire/welcome.html

National Oceanic and Atmospheric Administration (2002b) Ocean Explorer Explorations: Submarine Ring of Fire, Mission Plan - Explorer Ridge, 2002. URL: http://oceanexplorer.noaa.gov/explorations/02fire/background/plan/plan.html

Niu, Y., Collerson, K.D., Batiza, R., Wendt, J.I. and Regelous, M. (1999) Origin of enriched-type mid-ocean ridge basalt at ridges far from plumes: The East Pacific Rise at 11o20'N. *J. Geophys. Res.* **104**, 7067-7089.

Niu, Y., Regelous, M., Wendt, I.J., Batiza, R. and O'Hara, M.J. (2002) Geochemistry of near-EPR seamounts: Importance of source vs. process and the origin of enriched mantle component. *Earth Planet. Sci. Lett.* **199**, 327-345.

Nobre Silva, I.G., Weis, D., Barling, J. and Scoates, J.S. (2009) Leaching systematics and matrix elimination for the determination of high-precision Pb isotope compositions for ocean island basalts. *Geochem. Geophys. Geosyst.* **10**, doi: 10.1029/2009GC002537.

Nobre Silva, I.G., Weis, D. and Scoates, J.S. (2010) Effects of acid leaching on the Sr-Nd-Hf isotopic compositions of ocean island basalts. *Geochem. Geophys. Geosyst.* **11**, 20, doi: 10.1029/2010GC003176.

Perfit, M.R., Fornari, D.J., Smith, M.C., Bender, J.F., Langmuir, C.H. and Haymon, R.M. (1994) Small-scale spatial and temporal variations in mid-ocean ridge crest magmatic processes. *Geology* **22**, 375-379.

Pertermann, M. and Hirschmann, M.M. (2003) Partial melting experiments on a MORB-like pyroxenite between 2 and 3 GPa: Constraints on the presence of pyroxenite in basalt source regions from solidus location and melting rate. *J. Geophys. Res.* **108**, 2125.

Pertermann, M., Hirschmann, M.M., Hametner, K., Gunther, D. and Schmidt, M.W. (2004) Experimental determination of trace element partitioning between garnet and silica-rich liquid during anhydrous partial melting of a MORB-like eclogite. *Geochem. Geophys. Geosyst.* **5**.

PetDB (2015) Petrological database of the ocean floor. EarthChem, Lamont-Doherty Earth Observatory, Palisades, NY. URL: http://www.earthchem.org/petdb

Reynolds, J.R., Langmuir, C.H., Bender, J.F., Kastens, K.A. and Ryan, W.B.F. (1992) Spatial and temporal variability in the geochemistry of basalts from the East Pacific Rise. *Nature* **359**, 493-499.

Rhodes, J.M., Morgan, C. and Liias, R.A. (1990) Geochemistry of Axial Seamount lavas: magmatic relationship between the Cobb Hotspot and the Juan de Fuca Ridge. *J. Geophys. Res.* **95**, 12713-12734.

Riddihough, R.P. (1977) A model for recent plate interactions off Canada's west coast. *Can. J. Earth Sci.* **14**, 384-396.

Riddihough, R.P. (1984) Recent movements of the Juan de Fuca plate system. *J. Geophys. Res.* **89**, 6980-6994.

Riddihough, R.P., Currie, R.G. and Hyndman, R.D. (1980) The Dellwood Knolls and their role in the triple junction tectonics of northern Vancouver Island. *Can. J. Earth Sci.* **17**, 577-593.

Rohr, K.M.M. and Furlong, K.P. (1995) Ephemeral plate tectonics at the Queen Charlotte triple junction. *Geology* **23**, 1035-1038.

Salters, V.J.M., Mallick, S., Hart, S.R., Langmuir, C.H. and Stracke, A. (2011) Domains of depleted mantle: New evidence from hafnium and neodymium isotopes. *Geochem. Geophys. Geosyst.* **12**, 18, doi: 10.1029/2011GC003617.

Salters, V.J.M. and Stracke, A. (2004) Composition of the depleted mantle. *Geochem. Geophys. Geosyst.* **5**, doi: 10.1029/2003GC000597.

Schilling, J.-G. (1973) Iceland mantle plume: a geochemical study of the Reykjanes Ridge. *Nature* **242**, 565-571.

Schilling, J.-G. (1991) Fluxes and excess temperatures of mantle plumes inferred from their interaction with migrating mid-ocean ridges. *Nature* **352**, 397-403.

Schilling, J.-G., Zajac, M., Evans, R., Johnston, T., White, W., Devine, J.D. and Kingsley, R. (1983) Petrologic and geochemical variations along the Mid-Atlantic Ridge from 29oN to 73oN. *Amer. J. Sci.* **283**, 510-586.

Scott, S.D., Chase, R.L., Hannington, M.D., Michael, P.J., McConachy, T.F. and Shea, G.T. (1990) Sulphide deposits, tectonics and petrogenesis of Southern Explorer Ridge, Northeast Pacific Ocean, in: Malpas, J., Moores, E., Panayiotou, A., Xenophontos, C. (Eds.), *Ophiolites: Ocean Crustal Analogs*. Troodos Geological Survey Dept., Nicosia, pp. 719-733.

Shaw, D.M. (1970) Trace element fractionation during anatexis. *Geochim. Cosmochim. Acta* **34**, 237-243.

Smith, M.C., Perfit, M.R. and Jonasson, I.R. (1994) Petrology and geochemistry of basalts from the southern Juan de Fuca Ridge: controls on spatial and temporal evolution of mid-ocean ridge basalt. *J. Geophys. Res.* **99**, 4787-4812.

Stakes, D.S. and Franklin, J.M. (1994) Petrology of igneous rocks at Middle Valley, Juan de Fuca Ridge, in: Mottl, M.J., Davis, E.E., A.T., F., Slack, J.F. (Eds.), *Proceedings of the Ocean Drilling Program, Scientific Results 139*. Ocean Drilling Program, College Station, pp. 79-102.

Stix, J. and Gorton, M.P. (1992) Trace element analysis of ten U.S. Geological Survey rock standards by neutron activation using a low flux reactor. *Geostandards Newsletter* **16**, 21-26.

Stracke, A., Hofmann, A.W. and Hart, S.R. (2005) FOZO, HIMU, and the rest of the mantle zoo. *Geochem. Geophys. Geosyst.* **6**, doi: 10.1029/2004GC000824.

Sun, S.-s. and McDonough, W.F. (1989) Chemical and isotopic systematics of oceanic basalts: Implications for mantle composition and processes, in: Saunders, A.D., Norry, M.J. (Eds.), *Magmatism in the Ocean Basins*. Geological Society of London, Special Publication 42, London, pp. 313-345.

Thompson, G., Bryan, W.B., Ballard, R., Hamuro, K. and Melson, W.G. (1985) Axial processes along a segment of the East Pacific Rise, 10o-12oN. *Nature* **318**, 429-433.

Tunnicliffe, V., Botros, M., de Burgh, M.E., Dinet, A., Johnson, H.P., Juniper, S.K. and McDuff, R.E. (1986) Hydrothermal vents of Explorer Ridge, northeast Pacific. *Deep-sea Res.* **33**, 401-412.

Van Wagoner, N.A. and Leybourne, M.I. (1991) Evidence for magma mixing and a heterogeneous mantle on the West Valley segment of the Juan de Fuca Ridge. *J. Geophys. Res.* **96**, 16295-16318.

van Westrenen, W., Blundy, J.D. and Wood, B.J. (2001) High field strength element / rare earth element fractionation during partial melting in the presence of garnet: Implications for identification of mantle heterogeneities. *Geochem. Geophys. Geosyst.* **2**. doi: 2000GC000133

Waters, C.J., Sims, K.W.W., Perfit, M.R., Blichert-Toft, J. and Blusztajn, J. (2011) Perspective on the genesis of E-MORB from chemical and isotopic heterogeneity at 9-10oN East Pacific Rise. *J. Petrol.* **52**, 565-602, doi: 10.1093/petrology/egq091.

Weis, D., Kieffer, B., Hanano, D., Nobre Silva, I.G., Barling, J., Pretorius, W., Maerschalk, C. and Mattielli, N. (2007) Hf isotope compositions of U.S. Geological Survey reference materials. *Geochem. Geophys. Geosyst.* **8**, doi: 10.1029/2006GC001473.

Weis, D., Kieffer, B., Maerschalk, C., Barling, J., de Jong, J., Williams, G.A., Hanano, D., Pretorius, W., Mattielli, N., Scoates, J.S., Goolaerts, A., Friedman, R.M. and Mohoney, J.B. (2006) High-precision isotopic characterization of USGS reference materials by TIMS and MC-ICP-MS. *Geochem. Geophys. Geosyst.* **7**, Q08006, doi: 10.1029/2006GC001283.

Weis, D., Kieffer, B., Maerschalk, C., Pretorius, W. and Barling, J. (2005) High-precision Pb-Sr-Nd-Hf isotopic characterization of USGS BHVO-1 and BHVO-2 reference materials. *Geochem. Geophys. Geosyst.* **6**, Q02002.

Wendt, J.I., Regelous, M., Niu, Y., Hékinian, R. and Collerson, K.D. (1999) Geochemistry of lavas from the Garrett Transform Fault: Insights into mantle heterogeneity beneath the eastern Pacific. *Earth Planet. Sci. Lett.* **173**, 271-284.

White, W.M., Hofmann, A.W. and Puchelt, H. (1987) Isotope geochemistry of Pacific mid-ocean ridge basalt. *J. Geophys. Res.* **92**, 4881-4893.

White, W.M. and Schilling, J.-G. (1978) The nature and origin of geochemical variation in Mid-Atlantic Ridge basalts from the central North Atlantic. *Geochim. Cosmochim. Acta* **42**, 1501-1516.

White, W.M., Schilling, J.-G. and Hart, S.R. (1986) Strontium isotope geochemistry of the central north Atlantic: evidence for the Azores mantle plume. *Nature* **263**, 659.

Willbold, M. and Stracke, A. (2006) Trace element composition of mantle end-members: Implications for recycling of oceanic and upper and lower continental crust. *Geochem. Geophys. Geosyst.* **7**, Q04004, doi: 10.1029/2005GC001005.

Wilson, D.S., Hey, R.N. and Nishimura, C. (1984) Propagation as a mechanism of reorientation of the Juan de Fuca Ridge. *J. Geophys. Res.* **89**, 9215-9225.

Woodcock, J.P., Gill, J., Kela, J., Michael, P. and Ramos, F. (2006) Basalt geochemistry of the Endeavour Segment, Juan de Fuca Ridge, Amer. Geophys. Union Fall Meeting, San Francisco, pp. Paper B31B-1105.

Woodcock, J.P., Gill, J., Ramos, F. and Michael, P. (2007) Frequently shifting magma sources at Endeavour Segement, Juan de Fuca Ridge, Amer. Geophys. Union Fall Meeting, San Francisco, pp. Abs. V21B-0602.

**Table 1a. Major and Trace Element Data, Explorer Ridge Basalts**

| UBS Samples | ED | ED | ED | SER-N | SER-N | SER-AH | SER-AH |
|---|---|---|---|---|---|---|---|
| Cruise, Site | 79-06 | 79-06 | 79-06 | CASM5 | CR2 | CASM3 | CR2 |
| Fragment | 32-27 | 32-42 | 32-46 | D10 | D39-1 | 01 | D40-1 |
| Depth | 2375 | 2375 | 2375 | 2100 | 1985 | 1940 | 1773 |
| Latitude $^{o}$N | 49.9740 | 49.9740 | 49.9740 | 49.8700 | 49.8180 | 49.7680 | 49.7660 |
| Longitude $^{o}$W | 129.8830 | 129.8830 | 129.8830 | 130.1390 | 130.1790 | 130.2587 | 130.2690 |
| Sample Type | glass | glass | glass | glass | glass | glass | glass |
| $SiO_2$ | 50.15 | 51.12 | 50.99 | 51.24 | 50.79 | 50.75 | 51.74 |
| $TiO_2$ | 1.24 | 1.58 | 1.64 | 1.44 | 1.44 | 1.54 | 1.53 |
| $Al_2O_3$ | 15.83 | 15.03 | 15.16 | 14.46 | 14.32 | 14.86 | 14.73 |
| $FeO^t$ | 8.76 | 10.17 | 10.19 | 10.31 | 10.28 | 9.55 | 10.14 |
| MnO | 0.15 | 0.19 | 0.18 | 0.20 | 0.17 | 0.16 | 0.20 |
| MgO | 10.00 | 7.23 | 7.53 | 7.25 | 7.44 | 7.60 | 6.94 |
| CaO | 12.20 | 11.45 | 11.51 | 12.08 | 12.55 | 12.24 | 11.96 |
| $Na_2O$ | 2.17 | 2.48 | 2.47 | 2.24 | 2.22 | 2.30 | 2.45 |
| $K_2O$ | 0.302 | 0.442 | 0.444 | 0.406 | 0.297 | 0.489 | 0.526 |
| $P_2O_5$ | 0.143 | 0.219 | 0.206 | 0.184 | 0.148 | 0.195 | 0.226 |
| S | 0.054 | 0.105 | 0.100 | 0.099 | 0.103 | 0.097 | 0.106 |
| Cl | 0.015 | 0.027 | 0.031 | 0.020 | 0.017 | 0.023 | 0.030 |
| F | 0.02 | 0.03 | 0.03 | 0.02 | 0.01 | 0.04 | 0.02 |
| Total | 101.03 | 100.08 | 100.48 | 99.94 | 99.79 | 99.83 | 100.60 |
| $Mg/(Mg+Fe^{2+})$ | 0.7153 | 0.6100 | 0.6191 | 0.6073 | 0.6141 | 0.6365 | 0.6009 |
| V( ICP) | 225 | 327 | | 290 | 254 | | 319 |
| Cr (INAA) | 1180 | 295 | | 148 | 336 | | 78 |
| Co (INAA) | 52.8 | 42.8 | | 40.9 | 38.2 | | 41.9 |
| Ni (ICP) | 364 | 112 | | 60 | 73 | | 45 |
| Zn (ICP) | 69 | 88 | | 76 | 74 | | 82 |
| Rb (XRF) | 5 | 8 | | 7 | 5 | | 8 |
| Sr (XRF) | 166 | 166 | | 165 | 136 | | 206 |
| Y (XRF) | 22 | 29 | | 20 | 23 | | 26 |
| Zr (XRF) | 94 | 121 | | 95 | 73 | | 117 |
| Nb (XRF) | 10 | 18 | | 14 | 8 | | 18 |
| Ba (ICP) | 77 | 103 | | 97 | 56 | | 113 |
| La (INAA) | 6.99 | 11.29 | | 8.44 | 5.44 | | 12.33 |
| Ce (INAA) | 14.9 | 24.3 | | 18.7 | 12.1 | | 27.9 |
| Pr | | | | | | | |
| Nd (INAA) | 10.4 | 14.5 | | 9.3 | 7.5 | | 14.3 |
| Sm (INAA) | 2.82 | 3.90 | | 2.91 | 2.39 | | 3.80 |
| Eu (INAA) | 1.00 | 1.29 | | 1.06 | 0.83 | | 1.26 |
| Tb (INAA) | 0.54 | 0.70 | | 0.56 | 0.49 | | 0.70 |
| Dy | | | | | | | |

| | | | | | |
|---|---|---|---|---|---|
| Ho | | | | | |
| Er | | | | | |
| Tm (INAA) | 0.29 | 0.43 | 0.36 | 0.31 | |
| Yb (INAA) | 2.23 | 3.09 | 2.37 | 2.10 | 2.80 |
| Lu (INAA) | 0.34 | 0.44 | 0.37 | 0.32 | 0.41 |
| Hf (INAA) | 2.08 | 2.63 | 2.02 | 1.59 | 2.66 |
| Ta (INAA) | 0.56 | 1.03 | 0.82 | 0.49 | 1.27 |
| Th (INAA) | 0.77 | 1.14 | 0.73 | 0.54 | 1.32 |
| U (INAA) | 0.18 | 0.25 | 0.17 | 0.10 | 0.28 |
| Sc (INAA) | 37.3 | 40.9 | 41.9 | 39.3 | 43.8 |
| Y | | | | | |
| Zr | | | | | |
| Pb | | | | | |
| Rb | | | | | |
| Sr | | | | | |
| Nb | | | | | |
| Cs | | | | | |

Notes. ED = Explorer Deep, SER-N = SER North, SER-AH = SER Axial High, SER-Sem = Seminole Ridge, SER-S = SER South, ExpSmt = Explorer Seamount. See Table 1i for analytical details.

**Table 1b. Major and Trace Element Data, Explorer Ridge Basalts**

| UBS Samples | SER-AH | SER-AH | SER-AH | SER-AH | SER-AH | SER-AH | SER-AH |
|---|---|---|---|---|---|---|---|
| Cruise, Site | CR2 | CR2 | CR4 | CR3 | CR3 | CR3 | CR3 |
| Fragment | CV32 | CV34 | CV36-01 | D281-01 | D281-03 | D281-05 | D281-15 |
| Depth | 1941-2193 | - | 1830 | 1817 | 1803 | 1803 | 1745 |
| Latitude $^{o}$N | 49.74-49.77 | 49.76-49.78 | 49.7660 | 49.7590 | 49.7600 | 49.7590 | 49.7570 |
| Longitude $^{o}$W | 130.27-130.32 | 130.24-130.29 | 130.2700 | 130.2700 | 130.2710 | 130.2640 | 130.2600 |
| Sample Type | glass | glass | glass | glass | glass | glass | glass |
| $SiO_2$ | 51.45 | 50.71 | 51.65 | 50.88 | 50.74 | 50.63 | 51.01 |
| $TiO_2$ | 1.68 | 1.30 | 1.64 | 1.61 | 1.63 | 1.46 | 1.89 |
| $Al_2O_3$ | 14.45 | 15.00 | 14.90 | 14.27 | 14.44 | 14.47 | 13.92 |
| $FeO^t$ | 10.50 | 9.33 | 10.20 | 10.19 | 10.29 | 9.51 | 10.80 |
| MnO | 0.22 | 0.16 | 0.22 | 0.29 | 0.19 | 0.17 | 0.24 |
| MgO | 7.22 | 8.03 | 6.82 | 7.07 | 6.80 | 7.49 | 6.31 |
| CaO | 11.73 | 12.58 | 11.52 | 11.53 | 11.50 | 12.19 | 11.00 |
| $Na_2O$ | 2.73 | 2.24 | 2.57 | 2.50 | 2.62 | 2.33 | 2.72 |
| $K_2O$ | 0.231 | 0.368 | 0.548 | 0.492 | 0.490 | 0.443 | 0.578 |
| $P_2O_5$ | 0.174 | 0.181 | 0.231 | 0.224 | 0.214 | 0.215 | 0.238 |
| S | 0.118 | 0.102 | 0.118 | | 0.105 | | |
| Cl | 0.034 | 0.033 | 0.037 | 0.024 | 0.028 | 0.022 | |
| F | 0.01 | 0.02 | 0.05 | 0.02 | 0.04 | 0.04 | |
| Total | 100.55 | 100.05 | 100.50 | 99.10 | 99.07 | 98.97 | 98.71 |
| Mg/(Mg+Fe $^{2+}$) | 0.6021 | 0.6542 | 0.5953 | 0.6042 | 0.5924 | 0.6340 | 0.5624 |
| V( ICP) | | | | 326 | | 259 | |
| Cr (INAA) | | | | 60 | | 162 | |
| Co (INAA) | | | | 43.5 | | 36.9 | |
| Ni (ICP) | | | | 52 | | 55 | |
| Zn (ICP) | | | | 94 | | 69 | |
| Rb (XRF) | | | | 10 | | 7 | |
| Sr (XRF) | | | | 197 | | 211 | |
| Y (XRF) | | | | 28 | | 20 | |
| Zr (XRF) | | | | 129 | | 92 | |
| Nb (XRF) | | | | 18 | | 15 | |
| Ba (ICP) | | | | 127 | | 88 | |
| La (INAA) | | | | 12.03 | | 9.79 | |
| Ce (INAA) | | | | 26.0 | | 22.1 | |
| Pr | | | | | | | |
| Nd (INAA) | | | | 13.3 | | 11.7 | |
| Sm (INAA) | | | | 3.79 | | 3.02 | |
| Eu (INAA) | | | | 1.29 | | 1.07 | |
| | | | | | | | |
| Tb (INAA) | | | | 0.68 | | 0.57 | |
| Dy | | | | | | | |

| | | |
|---|---|---|
| Ho | | |
| Er | | |
| Tm (INAA) | | 0.43 |
| Yb (INAA) | 2.75 | 2.14 |
| Lu (INAA) | 0.39 | 0.34 |
| Hf (INAA) | 2.74 | 2.01 |
| Ta (INAA) | 1.13 | 0.92 |
| Th (INAA) | 1.22 | 0.94 |
| U (INAA) | 0.23 | 0.39 |
| Sc (INAA) | 43.3 | 39.0 |
| Y | | |
| Zr | | |
| Pb | | |
| Rb | | |
| Sr | | |
| Nb | | |
| Cs | | |

**Table 1c. Major and Trace Element Data, Explorer Ridge Basalts**

| UBS Samples | SER-AH | SER-AH | SER-AH | SER-AH | SER-AH | SER-AH | SER-AH |
|---|---|---|---|---|---|---|---|
| Cruise, Site | CR3 | CR3 | CR3 | CR3 | CR3 | CR4 | CR4 |
| Fragment | D281-15 | D281-17 | D283-01A | D284-05 | D284-16 | D320-01 | D321-02 |
| Depth | 1745 | 1804 | 1844 | 1771 | 1781 | 1812 | 1771 |
| Latitude $^{o}$N | 49.7570 | 49.7580 | 49.7570 | 49.7590 | 49.7590 | 49.7600 | 49.7590 |
| Longitude $^{o}$W | 130.2600 | 130.2610 | 130.2620 | 130.2570 | 130.2580 | 130.2560 | 130.2580 |
| Sample Type | glass | glass | glass | glass | glass | glass | glass |
| $SiO_2$ | 51.64 | 50.71 | 51.24 | 50.85 | 51.37 | 51.26 | 51.16 |
| $TiO_2$ | 1.96 | 1.85 | 1.89 | 1.89 | 1.91 | 1.95 | 1.82 |
| $Al_2O_3$ | 14.40 | 13.93 | 14.03 | 13.82 | 14.06 | 14.48 | 14.33 |
| $FeO^t$ | 10.98 | 10.76 | 10.63 | 10.88 | 10.74 | 10.91 | 10.95 |
| MnO | 0.18 | 0.20 | 0.21 | 0.29 | 0.22 | 0.21 | 0.18 |
| MgO | 6.50 | 6.28 | 6.31 | 6.26 | 6.33 | 6.60 | 6.42 |
| CaO | 11.06 | 11.11 | 10.80 | 11.02 | 11.03 | 11.13 | 11.11 |
| $Na_2O$ | 2.79 | 2.63 | 2.71 | 2.70 | 2.74 | 2.68 | 2.61 |
| $K_2O$ | 0.570 | 0.545 | 0.555 | 0.597 | 0.539 | 0.558 | 0.528 |
| $P_2O_5$ | 0.260 | 0.286 | 0.245 | 0.262 | 0.264 | 0.257 | 0.267 |
| S | 0.113 | | 0.111 | 0.109 | 0.129 | 0.123 | 0.123 |
| Cl | 0.032 | | 0.040 | 0.035 | 0.036 | 0.038 | 0.034 |
| F | 0.04 | | 0.04 | 0.04 | 0.04 | 0.06 | 0.04 |
| Total | 100.52 | 98.30 | 98.81 | 98.74 | 99.39 | 100.25 | 99.55 |
| $Mg/(Mg+Fe^{2+})$ | 0.5656 | 0.5622 | 0.5664 | 0.5587 | 0.5646 | 0.5711 | 0.5632 |
| V( ICP) | | 349 | | 351 | | 349 | 355 |
| Cr (INAA) | | 44 | | 41 | | 45 | 41 |
| Co (INAA) | | 44.6 | | 43.9 | | 43.0 | 42.8 |
| Ni (ICP) | | 37 | | 37 | | 40 | 40 |
| Zn (ICP) | | 96 | | 94 | | 100 | 91 |
| Rb (XRF) | | 9 | | 9 | | 9 | 9 |
| Sr (XRF) | | 197 | | 196 | | 198 | 198 |
| Y (XRF) | | 30 | | 29 | | 31 | 30 |
| Zr (XRF) | | 137 | | 136 | | 138 | 141 |
| Nb (XRF) | | 21 | | 20 | | 20 | 22 |
| Ba (ICP) | | 112 | | 139 | | 256 | 122 |
| La (INAA) | | 13.95 | | 14.08 | | 13.35 | 13.60 |
| Ce (INAA) | | 30.6 | | 31.8 | | 29.3 | 28.8 |
| Pr | | | | | | | |
| Nd (INAA) | | 17.1 | | 17.4 | | 16.4 | 17.8 |
| Sm (INAA) | | 4.59 | | 4.64 | | 4.36 | 4.46 |
| Eu (INAA) | | 1.55 | | 1.54 | | 1.46 | 1.45 |
| | | | | | | | |
| Tb (INAA) | | 0.85 | | 0.83 | | 0.79 | 0.79 |
| Dy | | | | | | | |

| | | | | | |
|---|---|---|---|---|---|
| Ho | | | | | |
| Er | | | | | |
| Tm (INAA) | 0.50 | 0.46 | 0.45 | 0.52 | |
| Yb (INAA) | 3.30 | 3.33 | 3.26 | | 3.20 |
| Lu (INAA) | 0.49 | 0.47 | 0.45 | | 0.45 |
| Hf (INAA) | 3.26 | 3.04 | 3.22 | | 3.14 |
| Ta (INAA) | 1.36 | 1.43 | 1.37 | | 1.30 |
| Th (INAA) | 1.39 | 1.53 | 1.25 | | 1.32 |
| U (INAA) | 0.37 | 0.34 | 0.33 | | 0.41 |
| Sc (INAA) | 46.0 | 45.5 | 43.1 | | 43.4 |
| Y | | | | | |
| Zr | | | | | |
| Pb | | | | | |
| Rb | | | | | |
| Sr | | | | | |
| Nb | | | | | |
| Cs | | | | | |

**Table 1d. Major and Trace Element Data, Explorer Ridge Basalts**

| UBS Samples | SER-AH | SER-S | SER-S | SER-S | SER-S | SER-S | SER-S |
|---|---|---|---|---|---|---|---|
| Cruise, Site | CR4 | CR1 | CR1 | CR1 | CR1 | CU1 | CU1 |
| Fragment | CV35-01 | D37-1 | D37-2 | D38-1 | D38-1 | D13-01 | D13-ut1 |
| Depth | 1817 | 1980 | 1980 | 1942 | 1942 | 2010 | 2010 |
| Latitude $^{o}$N | 49.7570 | 49.6960 | 49.6960 | 49.6940 | 49.6940 | 49.6400 | 49.6400 |
| Longitude $^{o}$W | 130.2800 | 130.3060 | 130.3060 | 130.3480 | 130.3480 | 130.3780 | 130.3780 |
| Sample Type | glass | glass | glass | glass | wr | glass | glass |
| $SiO_2$ | 51.17 | 51.28 | 50.96 | 50.77 | 50.67 | 49.74 | 51.05 |
| $TiO_2$ | 1.62 | 1.74 | 1.73 | 1.86 | 1.73 | 1.17 | 1.84 |
| $Al_2O_3$ | 14.91 | 14.59 | 14.39 | 14.56 | 14.71 | 16.75 | 14.55 |
| $FeO^t$ | 9.45 | 10.90 | 10.81 | 10.49 | 10.53 | 9.37 | 11.09 |
| MnO | 0.20 | 0.22 | 0.14 | 0.23 | 0.2 | 0.16 | 0.20 |
| MgO | 7.40 | 6.71 | 6.78 | 6.78 | 6.87 | 8.43 | 6.75 |
| CaO | 12.20 | 11.29 | 11.24 | 11.66 | 11.5 | 12.38 | 11.20 |
| $Na_2O$ | 2.37 | 2.79 | 2.70 | 2.86 | 2.8 | 2.53 | 2.99 |
| $K_2O$ | 0.485 | 0.406 | 0.402 | 0.355 | 0.36 | 0.161 | 0.345 |
| $P_2O_5$ | 0.223 | 0.237 | | 0.231 | 0.2 | 0.120 | 0.229 |
| S | 0.108 | 0.116 | | 0.116 | | 0.094 | 0.121 |
| Cl | 0.022 | 0.040 | | 0.035 | | 0.013 | 0.085 |
| F | 0.04 | 0.02 | | 0.02 | | 0.01 | 0.03 |
| Total | 100.20 | 100.33 | 99.15 | 99.96 | 99.15 | 100.92 | 100.49 |
| $Mg/(Mg+Fe^{2+})$ | 0.6328 | 0.5753 | 0.5799 | 0.5869 | 0.5894 | 0.6642 | 0.5726 |
| V( ICP) | | 338 | | 321 | 322 | 201 | 326 |
| Cr (INAA) | | 105 | | 155 | | 258 | 137 |
| Co (INAA) | | 42.8 | | 43.4 | | 45.0 | 43.3 |
| Ni (ICP) | | 47 | | 51 | 53 | 159 | 51 |
| Zn (ICP) | | 96 | | 96 | 97 | 62 | 92 |
| Rb (XRF) | | 6 | | 7 | 6 | 1 | 7 |
| Sr (XRF) | | 177 | | 169 | 166 | 168 | 160 |
| Y (XRF) | | 33 | | 34 | 32 | 20 | 39 |
| Zr (XRF) | | 139 | | 133 | 128 | 76 | 176 |
| Nb (XRF) | | 13 | | 12 | 13 | 4 | 12 |
| Ba (ICP) | | 75 | | 75 | 80 | 28 | 69 |
| La (INAA) | | 9.68 | | 9.91 | 8.88 | 3.60 | 9.47 |
| Ce (INAA) | | 24.0 | | 22.6 | 19.8 | 10.0 | 22.9 |
| Pr | | | | | | | |
| Nd (INAA) | | 17.0 | | 16.1 | 13.9 | 7.4 | 16.4 |
| Sm (INAA) | | 4.30 | | 4.39 | 4.25 | 2.36 | 4.95 |
| Eu (INAA) | | 1.42 | | 1.43 | 1.40 | 0.90 | 1.52 |
| | | | | | | | |
| Tb (INAA) | | 0.85 | | 0.87 | 0.82 | 0.55 | 0.99 |
| Dy | | | | | | | |

| | | | | | | |
|---|---|---|---|---|---|---|
| Ho | | | | | | |
| Er | | | | | | |
| Tm (INAA) | | | | 0.42 | 0.73 | |
| Yb (INAA) | 3.37 | 3.26 | 3.38 | 2.21 | | 4.29 |
| Lu (INAA) | 0.50 | 0.50 | 0.49 | 0.33 | | 0.65 |
| Hf (INAA) | 3.05 | 2.99 | 2.92 | 1.66 | | 3.83 |
| Ta (INAA) | 0.89 | 0.83 | 0.75 | 0.32 | | 0.70 |
| Th (INAA) | 0.91 | 0.92 | 0.79 | 0.28 | | 1.09 |
| U (INAA) | 0.23 | 0.18 | 0.16 | 0.04 | | 0.26 |
| Sc (INAA) | 44.6 | 44.4 | 42.9 | 36.2 | | 46.4 |
| Y | | | | | | |
| Zr | | | | | | |
| Pb | | | | | | |
| Rb | | | | | | |
| Sr | | | | | | |
| Nb | | | | | | |
| Cs | | | | | | |

**Table 1e. Major and Trace Element Data, Explorer Ridge Basalts**

| UBS Samples | SER-S | SER-S | NOAA Samples | SER-Sem | SER-Sem | SER-Sem | SER-Sem |
|---|---|---|---|---|---|---|---|
| Cruise, Site | CASM5 | CASM5 | Type | Rock Core | Rock Core | Rock Core | Rock Core |
| Fragment | D5 | D11 | Sample | RC01gl | RC02gl | RC03gl | RC04gl |
| Depth | 2300 | 2550 | Depth | 2040 | 2160 | 2060 | 2020 |
| Latitude $^{o}$N | 49.5600 | 49.4500 | Latitude | 49.75 | 49.7417 | 49.7517 | 49.7667 |
| Longitude $^{o}$W | 130.4190 | 130.4890 | Longitude | 130.1883 | 130.1933 | 130.22 | 130.2167 |
| Sample Type | glass | glass | Sample Type | glass | glass | glass | glass |
| $SiO_2$ | 51.86 | 50.51 | $SiO_2$ | 50.39 | 50.38 | 50.67 | 50.68 |
| $TiO_2$ | 1.60 | 1.47 | $TiO_2$ | 1.58 | 1.69 | 1.48 | 1.62 |
| $Al_2O_3$ | 14.67 | 14.68 | $Al_2O_3$ | 14.77 | 14.59 | 14.62 | 14.50 |
| $FeO^t$ | 10.09 | 10.33 | $FeO^t$ | 10.34 | 10.92 | 10.38 | 11.13 |
| MnO | 0.18 | 0.19 | MnO | 0.18 | 0.19 | 0.19 | 0.18 |
| MgO | 7.29 | 7.35 | MgO | 6.84 | 6.33 | 7.16 | 6.87 |
| CaO | 11.71 | 12.10 | CaO | 11.65 | 10.97 | 11.84 | 11.37 |
| $Na_2O$ | 2.54 | 2.45 | $Na_2O$ | 2.43 | 2.72 | 2.55 | 2.63 |
| $K_2O$ | 0.265 | 0.317 | $K_2O$ | 0.49 | 0.51 | 0.27 | 0.29 |
| $P_2O_5$ | 0.166 | 0.175 | $P_2O_5$ | | | | |
| S | 0.096 | 0.106 | S | | | | |
| Cl | 0.056 | 0.019 | Cl | 0.02 | 0.03 | 0.01 | 0.01 |
| F | 0.01 | 0.03 | F | 0.04 | 0.03 | 0.02 | 0.03 |
| Total | 100.54 | 99.72 | Total | 98.71 | 98.36 | 99.20 | 99.31 |
| $Mg/(Mg+Fe^{2+})$ | 0.6139 | 0.6103 | $Mg/(Mg+Fe^{2+})$ | 0.593 | 0.561 | 0.603 | 0.576 |
| V( ICP) | 238 | 286 | V (XRF) | 254 | 346 | 192 | >350 |
| Cr (INAA) | 263 | 258 | Cr | 139.25 | 42.18 | 74.86 | 97.82 |
| Co (INAA) | 38.4 | 41.4 | Co | 35.59 | 46.49 | 26.51 | 51.75 |
| Ni (ICP) | 88 | 62 | Ni | 59 | 41.01 | 35.87 | 63.48 |
| Zn (ICP) | 74 | 79 | Zn | 69.73 | 104.13 | 57.11 | 111.05 |
| Rb (XRF) | 4 | 5 | Rb | 8.35 | 11.88 | 3.86 | 7.33 |
| Sr (XRF) | 120 | 142 | Sr | 178.58 | 235.64 | 110.45 | 188.29 |
| Y (XRF) | 29 | 24 | Y | 23.51 | 33.76 | 18.44 | 39.03 |
| Zr (XRF) | 106 | 86 | Zr | 98.26 | 144.87 | 67.21 | 130.91 |
| Nb (XRF) | 8 | 10 | Nb | 15.64 | 22.74 | 6.75 | 12.94 |
| Ba (ICP) | 45 | 66 | Ba | 103.02 | 136.48 | 45.52 | 82 |
| La (INAA) | 5.65 | 6.87 | La (ICP-MS) | 10.61 | 15.36 | 5.12 | 9.84 |
| Ce (INAA) | 14.1 | 15.6 | Ce | 22.6 | 32.58 | 11.64 | 22.55 |
| Pr | | | Pr | 2.9 | 4.37 | 1.65 | 3.21 |
| Nd (INAA) | 9.8 | 10.7 | Nd | 12.69 | 18.67 | 7.49 | 15.57 |
| Sm (INAA) | 3.34 | 2.98 | Sm | 3.22 | 4.74 | 2.16 | 4.43 |
| Eu (INAA) | 1.08 | 1.04 | Eu | 1.2 | 1.84 | 0.87 | 1.72 |
| | | | Gd | 3.84 | 5.79 | 2.76 | 5.78 |
| Tb (INAA) | 0.70 | 0.61 | Tb | 0.62 | 0.92 | 0.48 | 1.02 |

| | | | | | | | |
|---|---|---|---|---|---|---|---|
| Dy | | | Dy | 4.1 | 6.07 | 3.18 | 6.42 |
| Ho | | | Ho | 0.84 | 1.25 | 0.69 | 1.38 |
| Er | | | Er | 2.31 | 3.74 | 2 | 3.84 |
| Tm (INAA) | 0.53 | 0.39 | Tm | 0.35 | 0.52 | 0.27 | 0.58 |
| Yb (INAA) | 2.97 | 2.59 | Yb | 2.22 | 3.4 | 1.69 | 3.64 |
| Lu (INAA) | 0.47 | 0.38 | Lu | 0.341 | 0.5 | 0.253 | 0.55 |
| Hf (INAA) | 2.61 | 1.98 | Hf | 2.45 | 3.72 | 1.73 | 3.46 |
| Ta (INAA) | 0.47 | 0.62 | Ta | 0.85 | 1.31 | 0.42 | 1.01 |
| Th (INAA) | 0.64 | 0.63 | Th | 1.09 | 1.59 | 0.46 | 0.84 |
| U (INAA) | 0.10 | 0.15 | U | 0.34 | 0.49 | 0.14 | 0.27 |
| Sc (INAA) | 36.0 | 42.3 | Sc | 34.25 | 47.68 | 27.68 | 52.62 |
| Y | | | Y | 23.51 | 33.76 | 18.44 | 39.03 |
| Zr | | | Zr | 98.26 | 144.87 | 67.21 | 130.91 |
| Pb | | | Pb | 1.98 | 1.51 | 0.87 | 1.94 |
| Rb | | | Rb | 8.35 | 11.88 | 3.86 | 7.33 |
| Sr | | | Sr | 178.58 | 235.64 | 110.45 | 188.29 |
| Nb | | | Nb | 15.64 | 22.74 | 6.75 | 12.94 |
| Cs | | | Cs | 0.12 | 0.14 | 0.07 | 0.09 |

**Table 1f. Major and Trace Element Data, Explorer Ridge Basalts**

| NOAA Samples | SER-Sem | SER-AH | SER-AH | SER-AH | SER-AH | SER-AH | SER-AH |
|---|---|---|---|---|---|---|---|
| Sample | Rock Core | Rock Core | ROPOS | ROPOS | ROPOS | ROPOS | ROPOS |
| BLC Designator | RC05 | RC06 | R665-RK0029 | R668-RK0005 | R665-RK0029 | R667-RK0001 | R670-RK0016 |
| Depth | 2015 | 1805 | 1742 | 1793 | 1742 | 1779 | 1804 |
| Latitude | 49.7583 | 49.7908 | 49.7675 | 49.7592 | 49.7675 | 49.7542 | 49.761 |
| Longitude | 130.2283 | 130.2417 | 130.2625 | 130.2592 | 130.2625 | 130.2766 | 130.265 |
| Sample Type | glass | glass | glass | glass | wr | wr | wr |
| $SiO_2$ | 50.81 | 50.10 | 50.15 | 50.50 | 49.32 | 49.17 | 50.52 |
| $TiO_2$ | 1.56 | 1.96 | 1.47 | 1.87 | 1.22 | 1.18 | 1.81 |
| $Al_2O_3$ | 14.71 | 14.55 | 15.11 | 14.45 | 17.01 | 17.78 | 14.60 |
| $FeO^t$ | 10.40 | 11.62 | 9.82 | 11.27 | 8.45 | 7.97 | 9.82 |
| MnO | 0.19 | 0.22 | 0.17 | 0.19 | 0.15 | 0.15 | 0.18 |
| MgO | 7.07 | 6.04 | 7.25 | 6.36 | 6.72 | 6.32 | 6.24 |
| CaO | 11.48 | 10.71 | 12.11 | 10.91 | 12.77 | 12.92 | 11.28 |
| $Na_2O$ | 2.58 | 2.82 | 2.43 | 2.73 | 2.13 | 2.14 | 2.68 |
| $K_2O$ | 0.34 | 0.57 | 0.45 | 0.56 | 0.40 | 0.43 | 0.58 |
| $P_2O_5$ | | | | | 0.18 | 0.17 | 0.26 |
| S | | | | | | | |
| Cl | 0.02 | 0.04 | 0.03 | 0.04 | | | |
| F | 0.05 | 0.03 | 0.03 | 0.00 | | | |
| Total | 99.21 | 98.66 | 99.02 | 98.89 | 98.35 | 98.52 | 97.97 |
| $Mg/(Mg+Fe^{2+})$ | 0.599 | 0.534 | 0.619 | 0.554 | 0.636 | 0.636 | 0.583 |
| V (XRF) | 324 | >350 | 260 | 348 | 261 | 255 | 360 |
| Cr | 88.69 | 44.92 | 140.29 | 33.03 | 163 | 136 | 42 |
| Co | 42.74 | 42.56 | 35.4 | 41.38 | 38 | 33 | 44 |
| Ni | 56.62 | 49.31 | 65.39 | 37.29 | 74 | 47 | 53 |
| Zn | 88.97 | 97.54 | 67.11 | 88.64 | 69 | 65 | 521 |
| Rb | 7.24 | 11.13 | 8.14 | 10.4 | 11 | 10 | 14 |
| Sr | 181.84 | 227.91 | 197.9 | 217.99 | 216 | 218 | 204 |
| Y | 30.67 | 34.18 | 22.53 | 31.63 | 23 | 21 | 32 |
| Zr | 114.47 | 147.19 | 93.46 | 137.56 | 83 | 78 | 124 |
| Nb | 12.98 | 22.58 | 16.01 | 21.51 | 14 | 13 | 19 |
| Ba | 81.08 | 129.06 | 96.91 | 119.79 | 112 | 109 | 139 |
| La (ICP-MS) | 9.52 | 15.2 | 10.67 | 14.01 | 11.25 | 9.99 | 14.86 |
| Ce | 21.03 | 32.17 | 22.28 | 29.75 | 24.08 | 21.62 | 31.94 |
| Pr | 2.98 | 4.4 | 2.94 | 3.95 | 3.203 | 2.898 | 4.353 |
| Nd | 13.31 | 19.9 | 12.38 | 17.74 | 13.34 | 12.25 | 18.8 |
| Sm | 3.8 | 4.72 | 2.97 | 4.41 | 3.26 | 2.99 | 4.69 |
| Eu | 1.44 | 1.8 | 1.21 | 1.68 | 1.176 | 1.109 | 1.641 |
| Gd | 4.9 | 5.53 | 3.48 | 5.24 | 3.955 | 3.571 | 5.532 |
| Tb | 0.82 | 0.92 | 0.58 | 0.88 | 0.684 | 0.595 | 0.923 |
| Dy | 5.28 | 5.96 | 3.92 | 5.29 | 4.072 | 3.593 | 5.773 |

| | | | | | | | |
|---|---|---|---|---|---|---|---|
| Ho | 1.09 | 1.23 | 0.78 | 1.17 | 0.87 | 0.795 | 1.271 |
| Er | 2.99 | 3.55 | 2.28 | 3.25 | 2.406 | 2.264 | 3.484 |
| Tm | 0.46 | 0.53 | 0.34 | 0.49 | 0.355 | 0.33 | 0.533 |
| Yb | 2.92 | 3.35 | 2.07 | 2.97 | 2.23 | 2.11 | 3.16 |
| Lu | 0.432 | 0.486 | 0.327 | 0.445 | 0.359 | 0.309 | 0.492 |
| Hf | 2.87 | 3.63 | 2.2 | 3.35 | 2.2 | 2.1 | 3.3 |
| Ta | 0.76 | 1.3 | 0.87 | 1.14 | 0.92 | 0.87 | 1.18 |
| Th | 0.86 | 1.5 | 1.04 | 1.33 | 1.07 | 1 | 1.4 |
| U | 0.27 | 0.51 | 0.35 | 0.42 | 0.347 | 0.368 | 1.361 |
| Sc | 43.82 | 42.68 | 37.24 | 41.99 | 43.91 | 40.54 | 48.94 |
| Y | 30.67 | 34.18 | 22.53 | 31.63 | 22.41 | 20.01 | 31.36 |
| Zr | 114.47 | 147.19 | 93.46 | 137.56 | 98.1 | 87.6 | 135.7 |
| Pb | 1.17 | 4.8 | 2.88 | 1.74 | 3.2 | 0.6 | 2.6 |
| Rb | 7.24 | 11.13 | 8.14 | 10.4 | 7.88 | 7.26 | 9.62 |
| Sr | 181.84 | 227.91 | 197.9 | 217.99 | 237.8 | 231.8 | 218.4 |
| Nb | 12.98 | 22.58 | 16.01 | 21.51 | 15.6 | 14.3 | 20.1 |
| Cs | 0.1 | 0.15 | 0.11 | 0.14 | 0.161 | 0.144 | 0.204 |

Notes. UBC samples: ED = Explorer Deep, SER = Southern Explorer Ridge. Major elements by electron microprobe on glass separates, in weight percent. Trace elements by XRF, ICP, or INAA as designated, in weight parts per million. NOAA samnples: Major element by fused-disk XRF (wr) or electron microprobe (gl) in weight percent. Trace elements by pressed-pellet XRF (V to Ba) and ICP-MS (La to Cs) in weight parts per million. Blank space = no data. $Mg/(Mg+Fe^{2+})$ calculated assuming $Fe^{2+}$ = 85% of total Fe. Major element totals do not include $H_2O$ or $CO_2$.

**Table 1g. Major and Trace Element Data, Explorer Seamount Basalts**

| UBS Samples | ExpSmt | ExpSmt | ExpSmt | ExpSmt | ExpSmt | ExpSmt | ExpSmt |
|---|---|---|---|---|---|---|---|
| Cruise, Site | HU81-17 | HU81-17 | HU81-17 | HU81-17 | HU81-17 | RC10 | RC10 |
| Fragment | ST31-ut1 | ST31-ut2 | ST32-102 | ST38b-ut1 | ST38b-ut2 | RD3-sr1 | RD3-sr2 |
| Depth | 1188 | 1188 | 900 | 1240 | 1240 | 1454 | 1454 |
| Latitude $^{o}$N | 49.0590 | 49.0590 | 49.0630 | 49.1210 | 49.1210 | 49.0580 | 49.0580 |
| Longitude $^{o}$W | 139.9400 | 139.9400 | 130.9410 | 131.0110 | 131.0110 | 130.9500 | 130.9500 |
| Sample Type | glass | glass | glass | glass | glass | glass | glass |
| $SiO_2$ | 48.31 | 49.10 | 48.47 | 48.26 | 48.26 | 48.07 | 48.58 |
| $TiO_2$ | 1.31 | 1.33 | 1.39 | 1.44 | 1.36 | 1.40 | 1.37 |
| $Al_2O_3$ | 17.25 | 17.34 | 17.14 | 17.15 | 16.96 | 16.91 | 17.23 |
| $FeO^t$ | 9.67 | 9.36 | 9.81 | 9.67 | 10.08 | 9.74 | 9.68 |
| MnO | 0.17 | 0.15 | 0.19 | 0.13 | 0.19 | 0.16 | 0.13 |
| MgO | 8.50 | 8.73 | 8.38 | 8.31 | 8.31 | 8.24 | 8.27 |
| CaO | 11.55 | 11.62 | 11.54 | 11.68 | 11.84 | 11.70 | 11.61 |
| $Na_2O$ | 2.86 | 2.83 | 3.00 | 2.92 | 3.01 | 3.04 | 3.08 |
| $K_2O$ | 0.054 | 0.059 | 0.057 | 0.033 | 0.049 | 0.062 | 0.057 |
| $P_2O_5$ | 0.111 | 0.107 | 0.102 | 0.104 | 0.112 | 0.116 | |
| S | 0.092 | 0.096 | 0.091 | 0.102 | 0.097 | 0.088 | |
| Cl | 0.011 | 0.012 | 0.014 | 0.007 | 0.003 | | |
| F | 0.01 | 0.00 | 0.02 | 0.01 | 0.02 | | |
| Total | 99.90 | 100.75 | 100.21 | 99.82 | 100.29 | 99.52 | 100.00 |
| $Mg/(Mg+Fe^{2+})$ | 0.6593 | 0.6724 | 0.6528 | 0.6540 | 0.6446 | 0.6505 | 0.6527 |
| V( ICP) | | 221 | 224 | | | | |
| Cr (INAA) | | 261 | 251 | | | | |
| Co (INAA) | | 46.5 | 47.5 | | | | |
| Ni (ICP) | | 127 | 118 | | | | |
| Zn (ICP) | | 76 | 81 | | | | |
| Rb (XRF) | | 2 | 1 | | | | |
| Sr (XRF) | | 176 | 182 | | | | |
| Y (XRF) | | 26 | 28 | | | | |
| Zr (XRF) | | 93 | 109 | | | | |
| Nb (XRF) | | 2 | 1 | | | | |
| Ba (ICP) | | 11 | 17 | | | | |
| La (INAA) | | 2.63 | 2.84 | | | | |
| Ce (INAA) | | 8.9 | 10.7 | | | | |
| Pr | | | | | | | |
| Nd (INAA) | | 8.7 | 9.0 | | | | |
| Sm (INAA) | | 2.95 | 3.19 | | | | |
| Eu (INAA) | | 1.10 | 1.19 | | | | |
| | | | | | | | |
| Tb (INAA) | | 0.62 | 0.68 | | | | |
| Dy | | | | | | | |

| | | |
|---|---|---|
| Ho | | |
| Er | | |
| Tm (INAA) | | 0.48 |
| Yb (INAA) | 2.96 | 2.94 |
| Lu (INAA) | 0.43 | 0.43 |
| Hf (INAA) | 2.03 | 2.43 |
| Ta (INAA) | 0.11 | 0.14 |
| Th (INAA) | 0.06 | 0.12 |
| U (INAA) | 0.08 | 0.02 |
| Sc (INAA) | 39.5 | 39.1 |
| Y | | |
| Zr | | |
| Pb | | |
| Rb | | |
| Sr | | |
| Nb | | |
| Cs | | |

**Table 1h. Major and Trace Element Data, Explorer Seamount Basalts**

| UBS Samples | ExpSmt | ExpSmt |
|---|---|---|
| Cruise, Site | RC10 | RC10 |
| Fragment | RD3-sr3 | RD3-sr4 |
| Depth | 1454 | 1454 |
| Latitude $^{o}$N | 49.0580 | 49.0580 |
| Longitude $^{o}$W | 130.9500 | 130.9500 |
| Sample Type | glass | glass |
| $SiO_2$ | 48.60 | 49.01 |
| $TiO_2$ | 1.42 | 1.45 |
| $Al_2O_3$ | 17.25 | 17.13 |
| $FeO^t$ | 9.32 | 9.78 |
| MnO | 0.17 | 0.19 |
| MgO | 8.47 | 8.30 |
| CaO | 11.47 | 11.52 |
| $Na_2O$ | 3.05 | 3.02 |
| $K_2O$ | 0.060 | 0.054 |
| $P_2O_5$ | 0.123 | |
| S | 0.092 | |
| Cl | 0.014 | |
| F | 0.01 | |
| Total | 100.05 | 100.46 |
| $Mg/(Mg+Fe^{2+})$ | 0.6666 | 0.6512 |
| V( ICP) | | 224 |
| Cr (INAA) | | 266 |
| Co (INAA) | | 46.7 |
| Ni (ICP) | | 127 |
| Zn (ICP) | | 75 |
| Rb (XRF) | | 1 |
| Sr (XRF) | | 194 |
| Y (XRF) | | 26 |
| Zr (XRF) | | 101 |
| Nb (XRF) | | 2 |
| Ba (ICP) | | 8 |
| La (INAA) | | 2.78 |
| Ce (INAA) | | 9.7 |
| Pr | | |
| Nd (INAA) | | 7.7 |
| Sm (INAA) | | 3.22 |
| Eu (INAA) | | 1.21 |
| Tb (INAA) | | 0.67 |

| | |
|---|---|
| Dy | |
| Ho | |
| Er | |
| Tm (INAA) | |
| Yb (INAA) | 2.86 |
| Lu (INAA) | 0.42 |
| Hf (INAA) | 2.20 |
| Ta (INAA) | 0.15 |
| Th (INAA) | 0.19 |
| U (INAA) | 0.12 |
| Sc (INAA) | 38.6 |
| Y | |
| Zr | |
| Pb | |
| Rb | |
| Sr | |
| Nb | |
| Cs | |

**Table 1i. Major and Trace Element Precisions, Explorer Basalts**

| UBC Samples | % Dev | % Dev | NOAA Samples | % Dev | % Dev |
|---|---|---|---|---|---|
| Sample Type | Glass | Whole rock | Sample Type | Glass | Whole rock |
| $SiO_2$ | 1 | 0.6 | $SiO_2$ | 2 | 0.6 |
| $TiO_2$ | 7 | 3.8 | $TiO_2$ | 5 | 1.6 |
| $Al_2O_3$ | 1 | 1.2 | $Al_2O_3$ | 2 | 0.6 |
| $FeO^t$ | 2 | 0.1 | $FeO^t$ | 2 | 0.3 |
| MnO | 22 | 4.5 | MnO | 10 | 2.9 |
| MgO | 1 | 1.4 | MgO | 5 | 3.4 |
| CaO | 1 | 0.8 | CaO | 2 | 1.8 |
| $Na_2O$ | 3 | 1.1 | $Na_2O$ | 5 | 1.5 |
| $K_2O$ | 2 | 1.5 | $K_2O$ | 5 | 0.9 |
| $P_2O_5$ | 6 | 3.1 | $P_2O_5$ | - | 1.4 |
| S | 5 | 16 | S | - | - |
| Cl | 7 | - | Cl | - | - |
| F | 83 | - | F | - | - |
| V( ICP) | | 2 | V (XRF) | | 5 |
| Cr (INAA) | | 5 | Cr | | 5 |
| Co (INAA) | | 1 | Co | | 4 |
| Ni (ICP) | | 2 | Ni | | 15 |
| Zn (ICP) | | 5 | Zn | | 1 |
| Rb (XRF) | | 6 | Rb | | 2 |
| Sr (XRF) | | 2 | Sr | | 2 |
| Y (XRF) | | 5 | Y | | 2 |
| Zr (XRF) | | 2 | Zr | | 1 |
| Nb (XRF) | | 10 | Nb | | 1 |
| Ba (ICP) | | 2 | Ba | | 4 |
| La (INAA) | | 3 | La (ICP-MS) | | 3 |
| Ce (INAA) | | 2 | Ce | | 3 |
| | | | Pr | | 4 |
| Nd (INAA) | | 7 | Nd | | 3 |
| Sm (INAA) | | 2 | Sm | | 3 |
| Eu (INAA) | | 2 | Eu | | 7 |
| | | | Gd | | 7 |
| Tb (INAA) | | 2 | Tb | | 6 |
| | | | Dy | | 4 |
| | | | Ho | | 3 |
| | | | Er | | 5 |
| Tm (INAA) | | 9 | Tm | | 7 |
| Yb (INAA) | | 5 | Yb | | 5 |
| Lu (INAA) | | 5 | Lu | | 5 |

| | | | |
|---|---|---|---|
| Hf (INAA) | 3 | Hf | 8 |
| Ta (INAA) | 5 | Ta | 15 |
| Th (INAA) | 1 | Th | 7 |
| U (INAA) | 15 | U | 6 |
| Sc (INAA) | 2 | Sc | 2 |
| | | Y | 2 |
| | | Zr | 2 |
| | | Pb | 2 |
| | | Rb | 2 |
| | | Sr | 1 |
| | | Nb | 2 |
| | | Cs | 4 |

Notes. ED = Explorer Deep, SER-N = SER North, SER-AH = SER Axial High, SER-Sem = Seminole Ridge, SER-S = SER South, ExpSmt = Explorer Seamount. UBC/UT samples: Major elements by electron microprobe on glass separates, in weight percent. Trace elements by XRF, ICP, or INAA as designated, in weight parts per million. NOAA samnples: Major element by fused-disk XRF (wr) or electron microprobe (gl) in weight percent. Trace elements by pressed-pellet XRF (V to Ba) and ICP-MS (La to Cs) in weight parts per million. Blank space = no data. $Mg/(Mg+Fe^{2+})$ calculated assuming $Fe^{2+}$ = 85% of total Fe. Major element totals do not include $H_2O$ or $CO_2$.

| Table 1j. Major and Trace Element Standards Precisions, Explorer Basalts | | | | | | |
|---|---|---|---|---|---|---|
| UBC/UT Samples | | | | NOAA Samples | | |
| Sample | VG-2 Glass | 1-sigma | VG-2 (pub) | Sample Type | VG-2 Glass | |
| $SiO_2$ | 50.89 | 0.52 | 50.81 | $SiO_2$ | 50.30 | |
| $TiO_2$ | 1.84 | 0.15 | 1.85 | $TiO_2$ | 1.95 | |
| $Al_2O_3$ | 14.02 | 0.12 | 14.06 | $Al_2O_3$ | 13.51 | |
| $FeO^t$ | 11.72 | 0.20 | 11.84 | $FeO^t$ | 11.23 | |
| MnO | 0.21 | 0.05 | 0.22 | MnO | 0.20 | |
| MgO | 6.97 | 0.10 | 6.71 | MgO | 6.66 | |
| CaO | 11.06 | 0.15 | 11.12 | CaO | 11.17 | |
| $Na_2O$ | 2.63 | 0.08 | 2.62 | $Na_2O$ | 2.64 | |
| $K_2O$ | 0.199 | 0.008 | 0.19 | $K_2O$ | 0.21 | |
| $P_2O_5$ | 0.207 | 0.012 | 0.20 | $P_2O_5$ | 0.16 | |
| S | 0.122 | 0.005 | | S | 0.12 | |
| Cl | 0.0299 | 0.0022 | | Cl | 0.03 | |
| F | 0.0166 | 0.0128 | | F | - | |
| | BIR-1 | UTB-1 | BHVO-1 | | BIR-1 | BHVO-2 |
| V( ICP) | | 41 (35) | | V (XRF) | 326 (321) | 320 (318) |
| Cr (INAA) | 427 (392) | | 295 (288) | Cr | 398 (392) | 292 (287) |
| Co (INAA) | 52.6 (52.2) | | 43.8 (44.9) | Co | 54.5 (52.2) | 45.0 (44.9) |
| Ni (ICP) | | 26 (25) | | Ni | 176 (169) | 120 (120) |
| Zn (ICP) | | 150 (135) | | Zn | 74 (70) | 101 (104) |
| Rb (XRF) | | 32.8 (32.5) | | Rb | | |
| Sr (XRF) | | 309 (307) | | Sr | | |
| Y (XRF) | | 43 (43) | | Y | | |
| Zr (XRF) | | 204 (200) | | Zr | | |
| Nb (XRF) | | 14.9 (15.5) | | Nb | | |
| Ba (ICP) | | 509 (530) | | Ba | 6.7 (6.75) | 130 (131) |
| La (INAA) | 0.52 (0.63) | 26.9 (26.6) | 15 (15.44) | La (ICP-MS) | 0.65 (0.63) | 15.19 (15.2) |
| Ce (INAA) | 2.10 (1.92) | 61.7 (60.5) | 38 (38.08) | Ce | 1.74 (1.92) | 36.6 (37.5) |
| | | | | Pr | 0.39 (0.37) | 5.28 (5.34) |
| Nd (INAA) | 1.8 (2.4) | 34.1 (32.0) | 23 (24.78) | Nd | 2.55 (2.40) | 24.64 (24.27) |
| Sm (INAA) | 1.10 (1.11) | 8.27 (8.0) | 6.0 (6.17) | Sm | 1.18 (1.11) | 6.09 (6.02) |
| Eu (INAA) | 0.52 (0.52) | 2.47 (2.4) | 2.0 (2.05) | Eu | 0.49 (0.52) | 2.06 (2.04) |
| | | | | Gd | 1.84 (1.81) | 6.19 (6.21) |
| Tb (INAA) | 0.32 (0.36) | 1.25 (1.3) | 1.0 (0.94) | Tb | | 0.92 (0.94) |
| | | | | Dy | 2.46 (2.54) | 5.33 (5.28) |
| | | | | Ho | 0.59 (0.57) | 0.97 (0.99) |
| | | | | Er | 1.68 (1.68) | 2.50 (2.51) |
| Tm (INAA) | No data | 0.7 (0.6) | | Tm | | 0.34 (0.34) |

| | | | | | | |
|---|---|---|---|---|---|---|
| Yb (INAA) | 1.77 (1.63) | 4.14 (4,0) | 2.0 (1.99) | Yb | 1.57 (1.63) | 1.96 (1.99) |
| Lu (INAA) | 0.26 (0.25) | 0.61 (0.6) | 0.31 (0.28) | Lu | 0.26 (0.25) | 0.27 (0.28) |
| Hf (INAA) | 0.62 (0.58) | 4.73 (4.7) | 4.3 (4.44) | Hf | 0.56 (0.58) | 4.35 (4.47) |
| Ta (INAA) | 0.03 (0.04) | 1.02 (1.0) | 1.2 (1.17) | Ta | | 1.13 (1.15) |
| Th (INAA) | 0.10 (0.03) | 4.33 (4.3) | 1.25 (1.23) | Th | | 1.19 (1.22) |
| U (INAA) | No data | 1.0 (1.0) | 0.33 (0.42) | U | | 0.41 (0.41) |
| Sc (INAA) | 45 (43) | 39.1 (39) | 32.2 (31.4) | Sc | 45.42 (43) | 32.3 (31.8) |
| | | | | Y | 16.6 (15.6) | 25.8 (25.9) |
| | | | | Zr | 15.3 (14.8) | 171 (171) |
| | | | | Pb | 3.10 (3.04) | 1.66 (1.65) |
| | | | | Rb | | 9.26 (9.30) |
| | | | | Sr | 107 (109) | 385 (394) |
| | | | | Nb | 0.66 (0.55) | 17.4 (18.1) |
| | | | | Cs | | 0.10 (0.10) |

Notes. UBC samples: Major elements by electron microprobe on glass separates, in weight percent. VG-2 was run as a calibration standard ("pub" are published values of Jarosewich et al., 1980). Trace elements by XRF, ICP, or INAA as designated, in weight parts per million. NOAA samnples: Major element by fused-disk XRF (wr) or electron microprobe (gl) in weight percent. XRF analyses are calibrated using certified international rock standards. Glass analyses by microprobe are calibrated using a series of natural and synthetic minerals, and VG-2 is sometimes run as an unknown. Values in parentheses are "accepted" values for BIR-1 and BHVO-2 from Jochum et al. (2016) and for UTB-1 and BHVO-1 from Stix and Gorton (1992).

**Table 2a. Isotopic Data for Explorer Basalts.**

| Cruise | Sample | $^{87}Sr/^{86}Sr$ | $^{143}Nd/^{144}Nd$ | $\varepsilon_{Nd}$ | $^{206}Pb/^{204}Pb$ TIMS | $^{207}Pb/^{204}Pb$ TIMS | $^{208}Pb/^{204}Pb$ TIMS |
|---|---|---|---|---|---|---|---|
| 79-06 | 32-42 | 0.702638 | 0.513080 | 8.62 | | | |
| 79-06 | 32-27 | 0.702694 | 0.513081 | 8.64 | | | |
| CASM5 | D10 | 0.702735 | 0.513064 | 8.31 | | | |
| CR2 | D39-1 | 0.702673 | 0.513064 | 8.31 | | | |
| CR2 | D40-1 | 0.702694 | 0.513067 | 8.37 | | | |
| CR4 | D320-01 | 0.702679 | 0.513107 | 9.15 | | | |
| CR3 | D281-01 | 0.702662 | 0.513081 | 8.64 | | | |
| CR3 | D284-05 | 0.702659 | nd | | | | |
| CR3 | D281-05 | 0.702699 | 0.513032 | 7.69 | | | |
| CR1 | D37-1 | 0.702592 | 0.513053 | 8.10 | | | |
| CR1 | D38-1 | 0.702509 | 0.513187 | 10.71 | | | |
| CU1 | D13-ut1 | 0.702630 | 0.513129 | 9.58 | | | |
| CU1 | D13-01 | 0.702593 | 0.513128 | 9.56 | | | |
| CASM5 | D5 | 0.702553 | 0.513165 | 10.28 | | | |
| CASM5 | D11 | 0.702638 | 0.513106 | 9.13 | | | |
| HU81-17 | ST32-102 | 0.702386 | 0.513239 | 11.72 | | | |
| HU81-17 | ST31-ut2 | 0.702487 | 0.513197 | 10.9 | | | |
| NOAA | RC02 | 0.702965 | 0.513024 | 7.53 | 19.171 | 15.539 | 38.417 |
| NOAA | RC04 | 0.702775 | 0.513032 | 7.69 | 19.066 | 15.509 | 38.262 |
| NOAA | RC05 | 0.702713 | 0.513060 | 8.23 | 19.099 | 15.540 | 38.335 |
| NOAA | R665-RK0029gl | 0.702702 | 0.513004 | 7.14 | 18.976 | 15.534 | 38.326 |
| NOAA | R668-RK0005gl | 0.702866 | 0.513044 | 7.92 | 19.095 | 15.501 | 38.312 |
| NOAA | R667-RK0001 wr | 0.702727 | 0.513056 | 8.15 | 19.173 | 15.539 | 38.412 |
| NOAA | R670-RK0016 wr | nd | 0.513091 | 8.84 | 19.110 | 15.533 | 38.355 |
| Precision | | 0.000019 | 0.000015 | 0.30 | 0.011 | 0.012 | 0.042 |

Notes: $\varepsilon_{Nd}$ values calculated relative to a $^{143}Nd/^{144}Nd$ for CHUR of 0.512638. Sr, Nd and Pb isotopic ratios determined by TIMS at Carleton University. "nd" = no successful mass spectrometer run.

**Table 2b. Isotopic Data for Explorer Basalts.**

| Cruise | Sample | $^{176}Hf/^{177}Hf$ | $\varepsilon_{Hf}$ | $^{206}Pb/^{204}Pb$ Nu | $^{207}Pb/^{204}Pb$ Nu | $^{208}Pb/^{204}Pb$ Nu |
|---|---|---|---|---|---|---|
| 79-06 | 32-42 | 0.283092 | 11.31 | 19.2142 | 15.5446 | 38.4436 |
| 79-06 | 32-27 | 0.283030 | 9.14 | 19.0835 | 15.5467 | 38.3608 |
| CASM5 | D10 | 0.283009 | 8.36 | 19.0840 | 15.5476 | 38.3941 |
| CR2 | D39-1 | 0.283042 | 9.53 | 19.1670 | 15.5564 | 38.4172 |
| CR2 | D40-1 | 0.283065 | 10.36 | 19.1924 | 15.5507 | 38.4512 |
| CR4 | D320-01 | 0.283090 | 11.24 | 19.1352 | 15.5363 | 38.3854 |
| CR3 | D281-01 | | | 19.2614 | 15.5654 | 38.4302 |
| CR3 | D284-05 | 0.283094 | 11.40 | 19.1439 | 15.5414 | 38.4064 |
| CR3 | D281-05 | 0.283062 | 10.24 | 19.2028 | 15.5519 | 38.4621 |
| CR1 | D37-1 | 0.283099 | 11.57 | 18.9762 | 15.5234 | 38.2508 |
| CR1 | D38-1 | 0.283102 | 11.66 | | | |
| CU1 | D13-ut1 | 0.283112 | 12.03 | 18.8886 | 15.5034 | 38.1619 |
| CU1 | D13-01 | 0.283100 | 11.60 | 18.8269 | 15.4929 | 38.1159 |
| CASM5 | D5 | 0.283140 | 13.00 | 18.9022 | 15.5188 | 38.2293 |
| CASM5 | D11 | 0.283064 | 10.33 | 19.0354 | 15.5502 | 38.3263 |
| HU81-17 | ST32-102 | 0.283158 | 13.63 | | | |
| HU81-17 | ST31-ut2 | 0.283069 | 10.49 | 18.4060 | 15.4380 | 37.7610 |
| Precision | | 0.000010 | 0.35 | 0.0013 | 0.0015 | 0.0040 |

Notes: $\varepsilon_{Hf}$ values calculated relative to a $^{176}Hf/^{177}Hf$ for CHUR of 0.282772. Pb and Hf isotopic ratios determined by Nu MC-ICP-MS at the University of British Columbia.

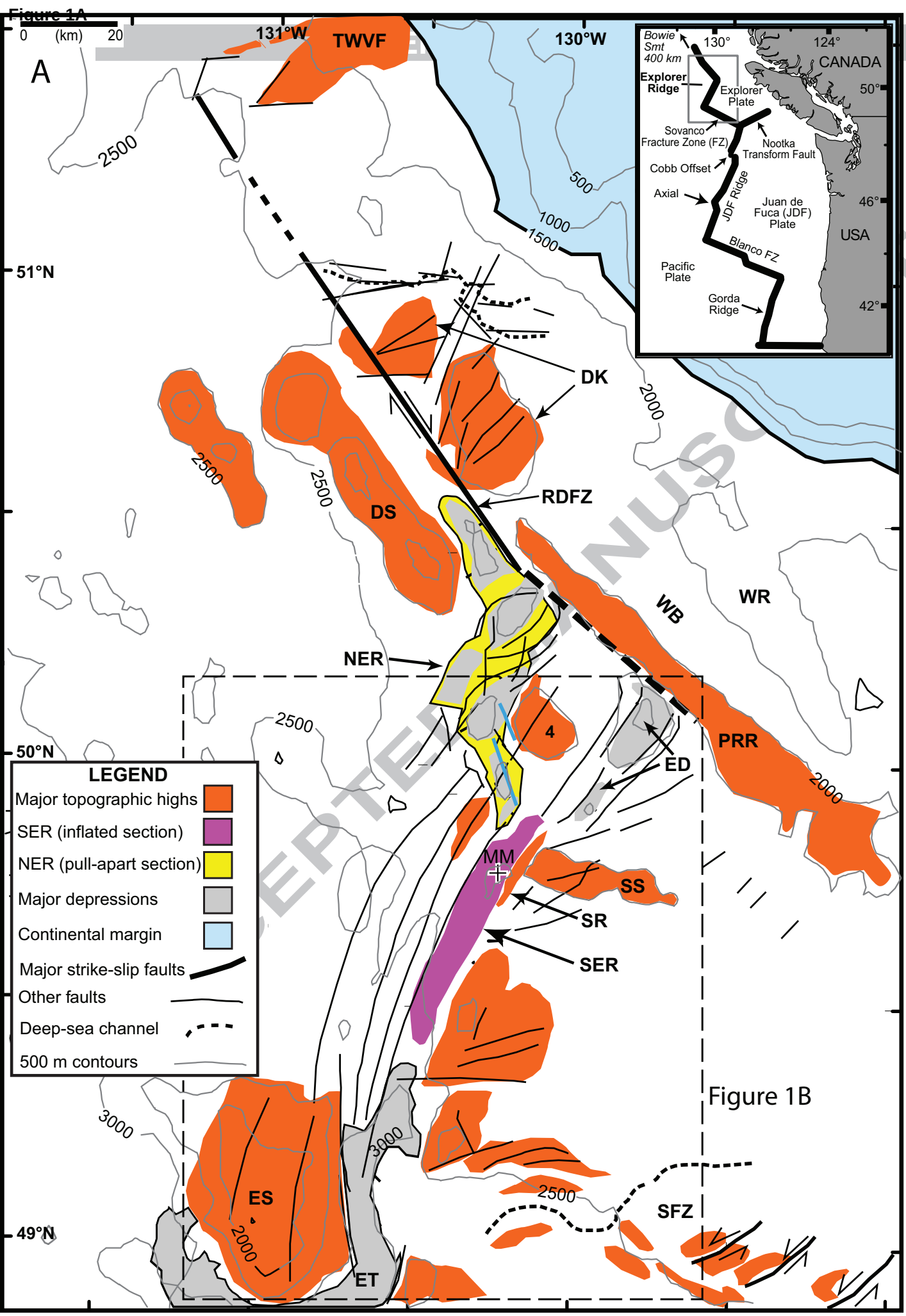
Figure 1A
0 (km) 20
A
131°W
130°W
TWVF
2500
500
1000
1500
2000
51°N
50°N
49°N
DK
RDFZ
DS
WB
WR
NER
4
PRR
ED
MM
SS
SR
SER
ES
ET
SFZ
3000
Bowie Smt 400 km
Explorer Ridge
Explorer Plate
Sovanco Fracture Zone (FZ)
Nootka Transform Fault
Cobb Offset
Axial
JDF Ridge
Juan de Fuca (JDF) Plate
Blanco FZ
Pacific Plate
Gorda Ridge
130°
124°
CANADA
50°
46°
USA
42°
LEGEND
Major topographic highs
SER (inflated section)
NER (pull-apart section)
Major depressions
Continental margin
Major strike-slip faults
Other faults
Deep-sea channel
500 m contours
Figure 1B

Figure 1A

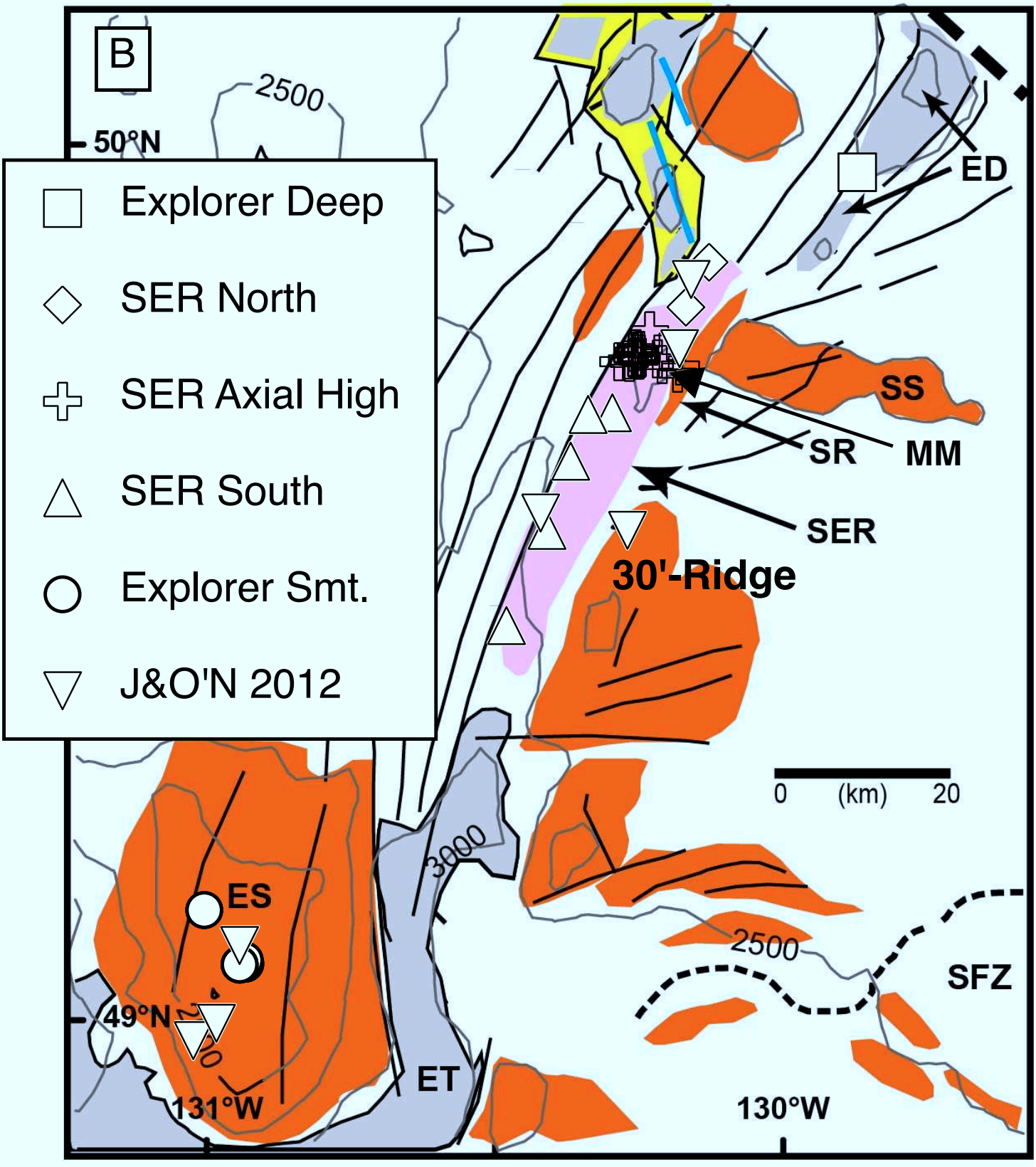


Figure 1B

Figure 2

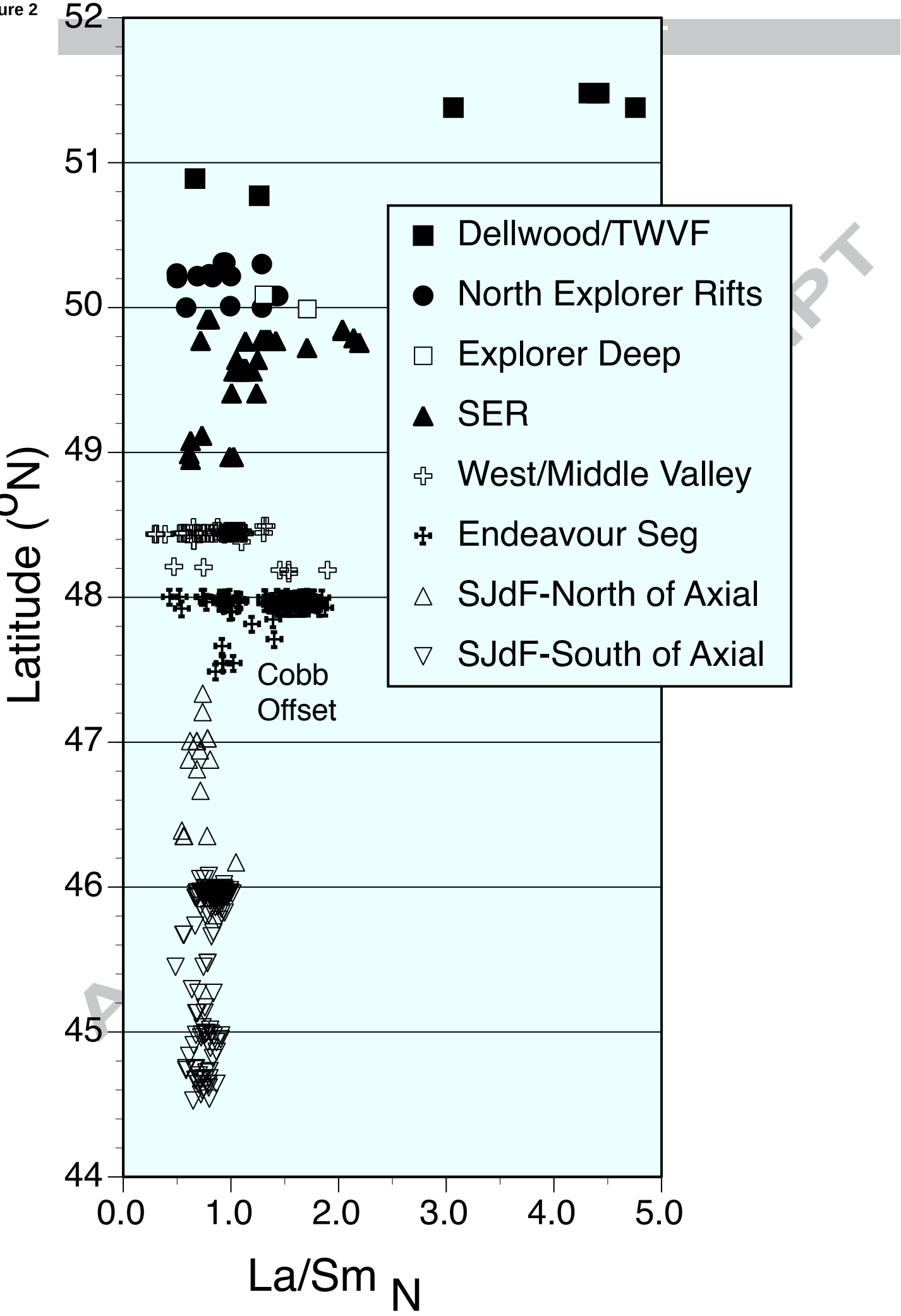
52
51
50
49
48
47
46
45
44
Latitude (°N)
0.0
1.0
2.0
3.0
4.0
5.0
La/Sm N
Dellwood/TWVF
North Explorer Rifts
Explorer Deep
SER
West/Middle Valley
Endeavour Seg
SJdF-North of Axial
SJdF-South of Axial
Cobb
Offset

Figure 3



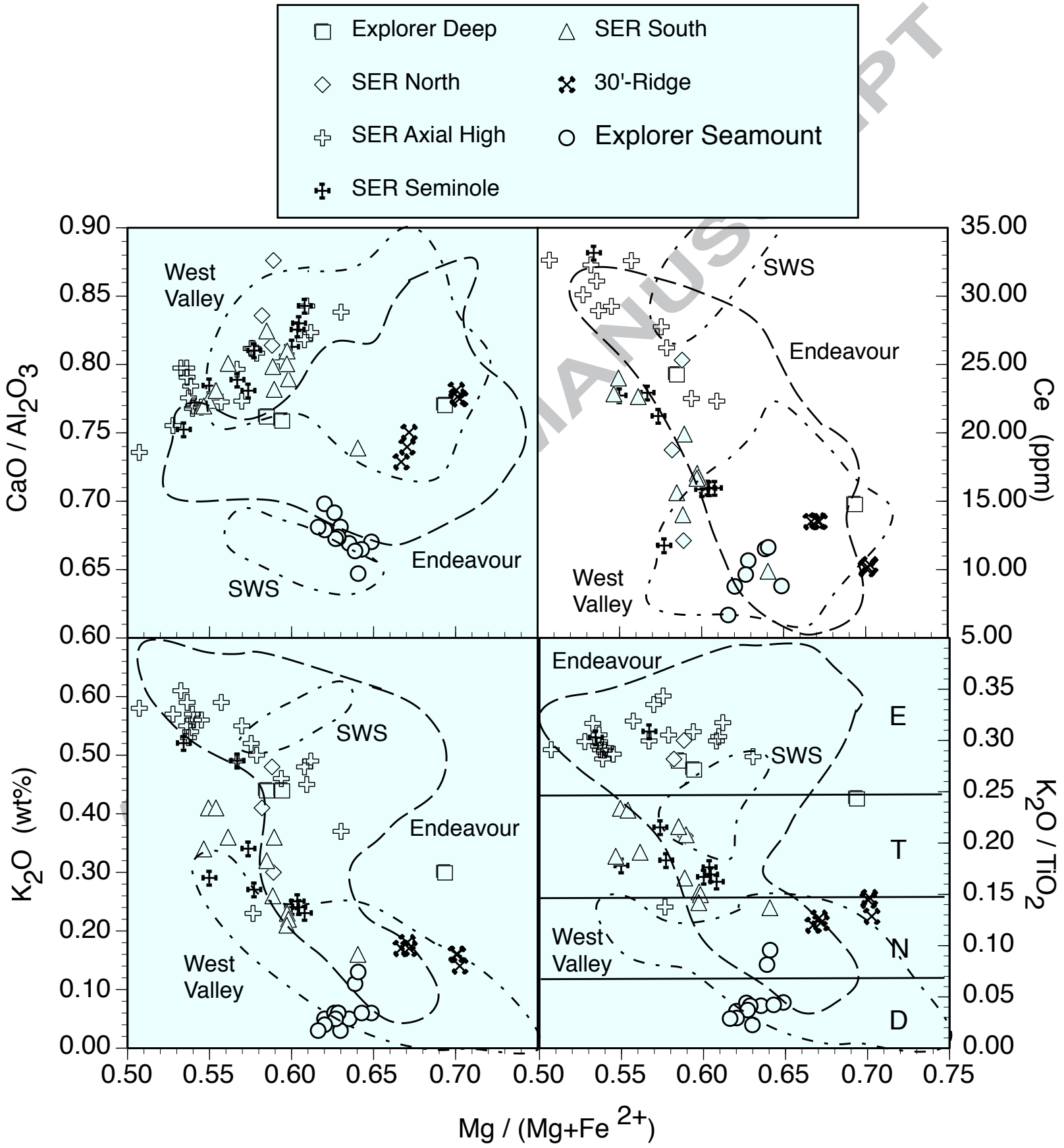

Figure 4



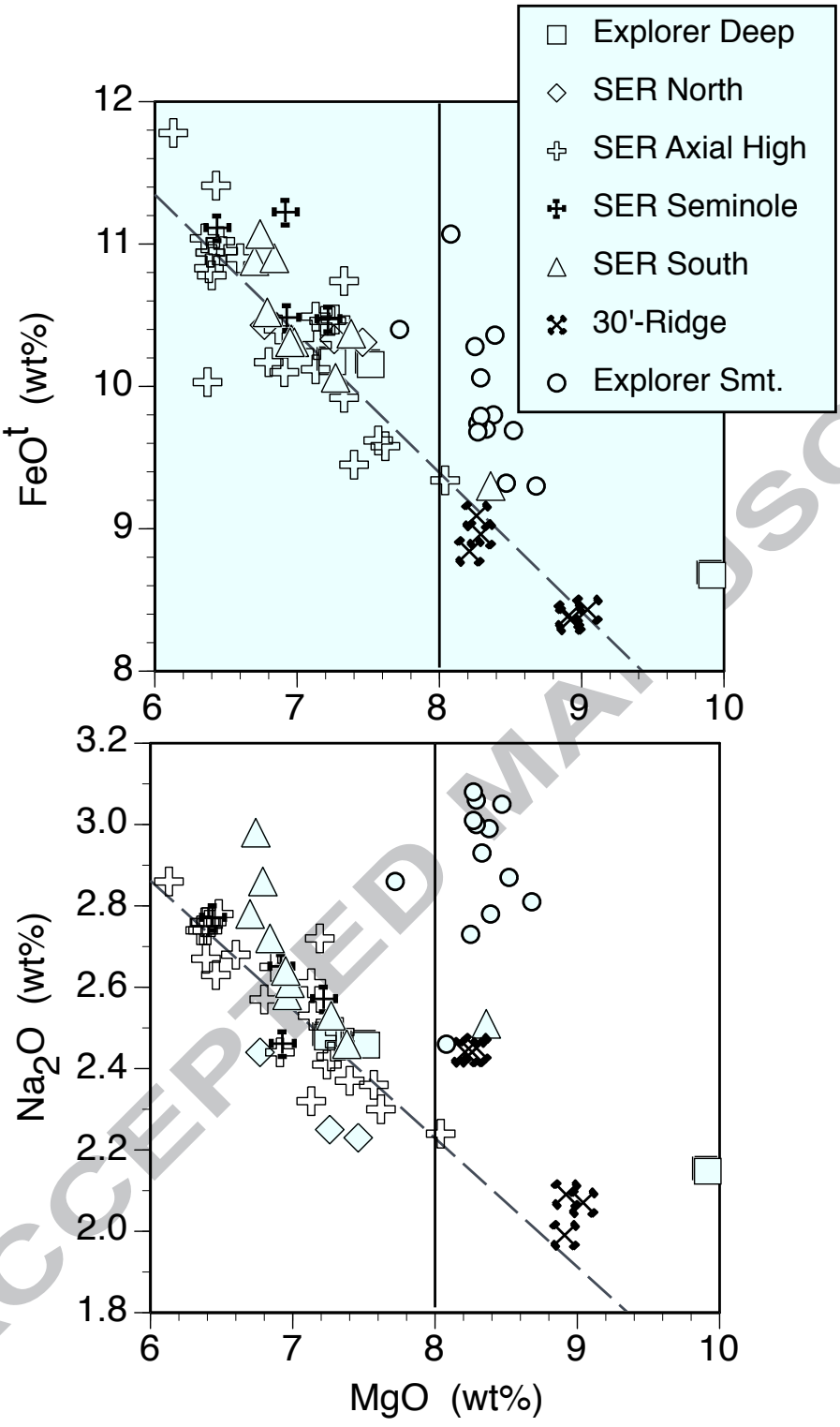

Figure 5



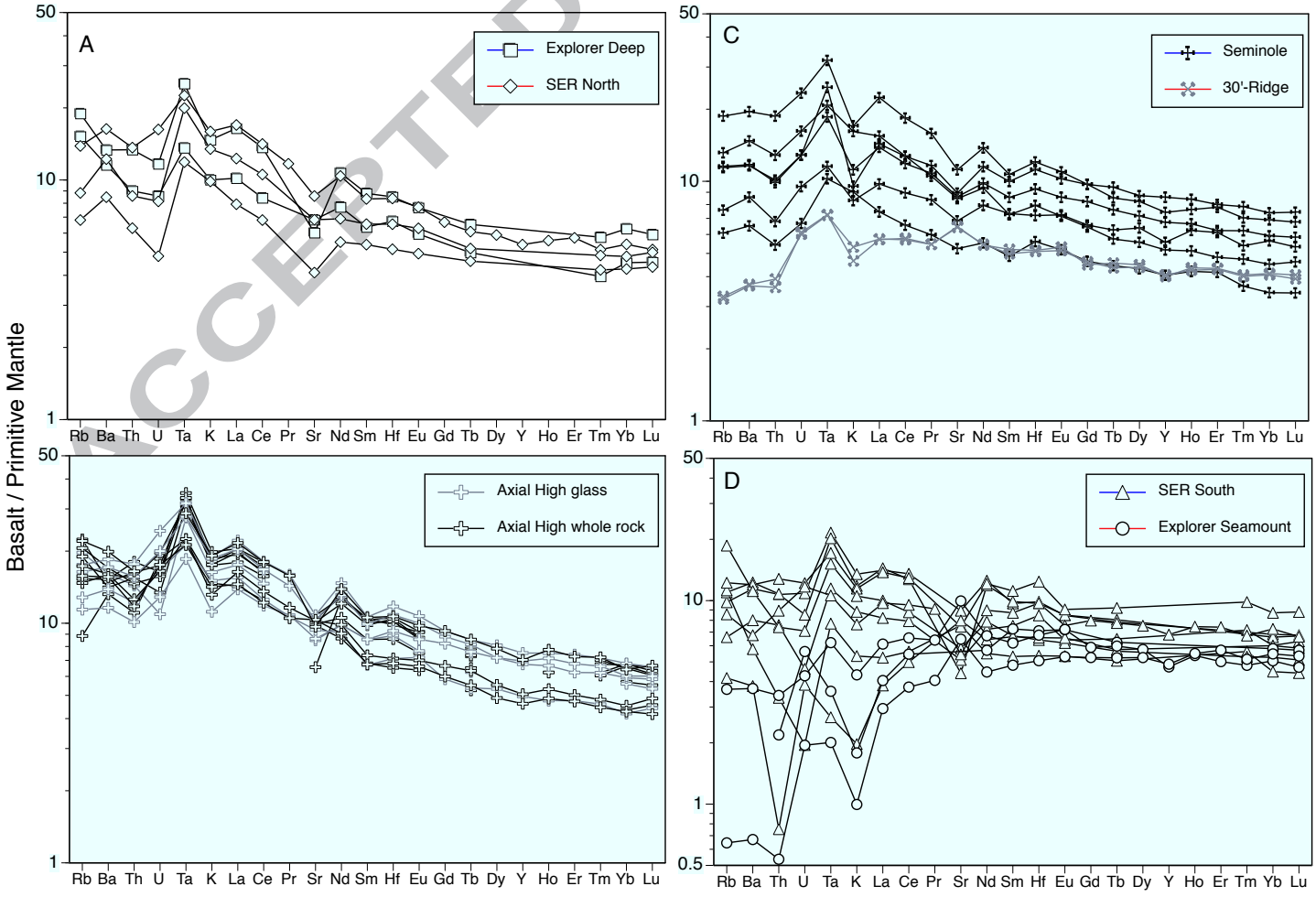

Figure 6



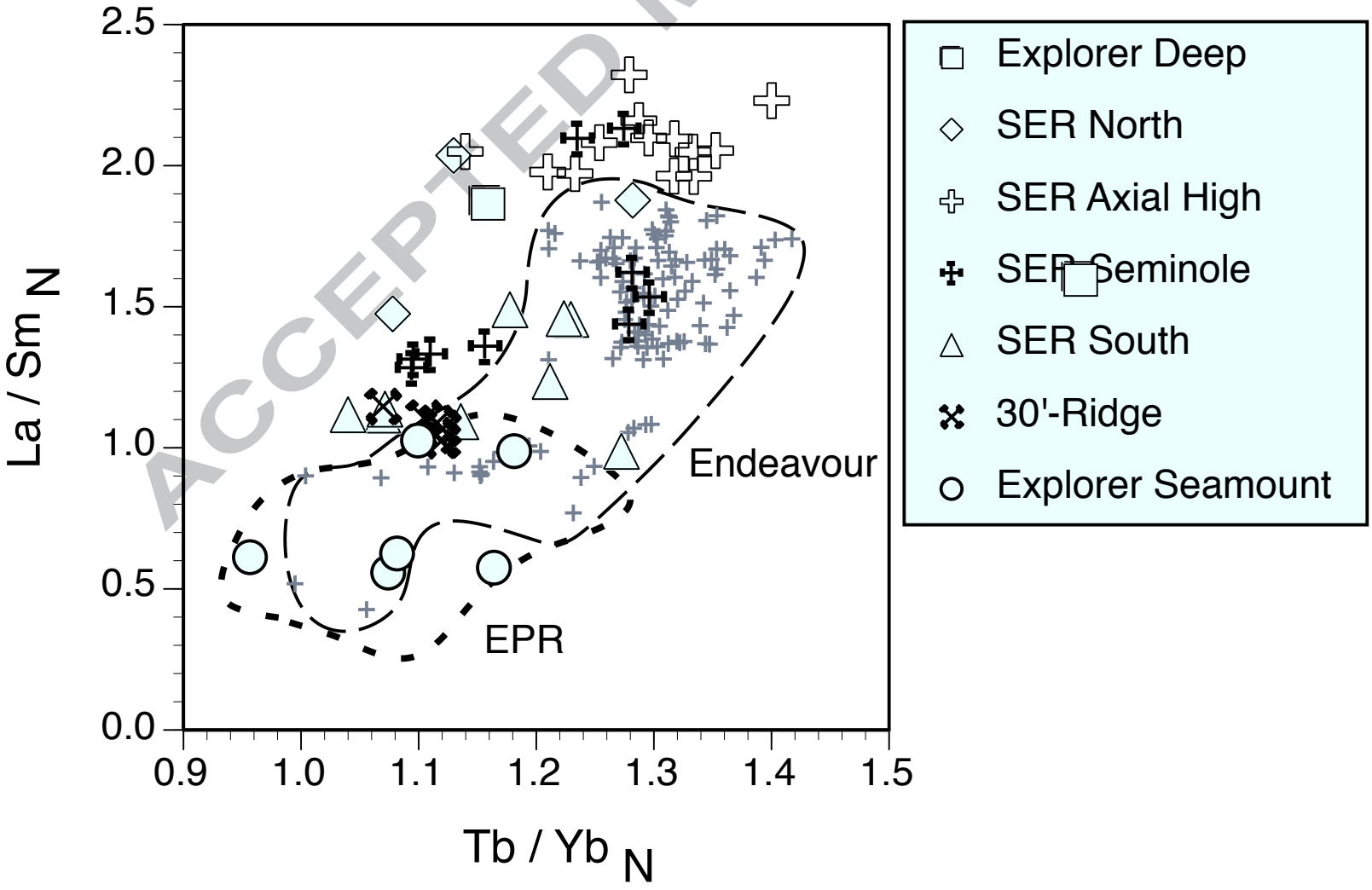

Figure 7



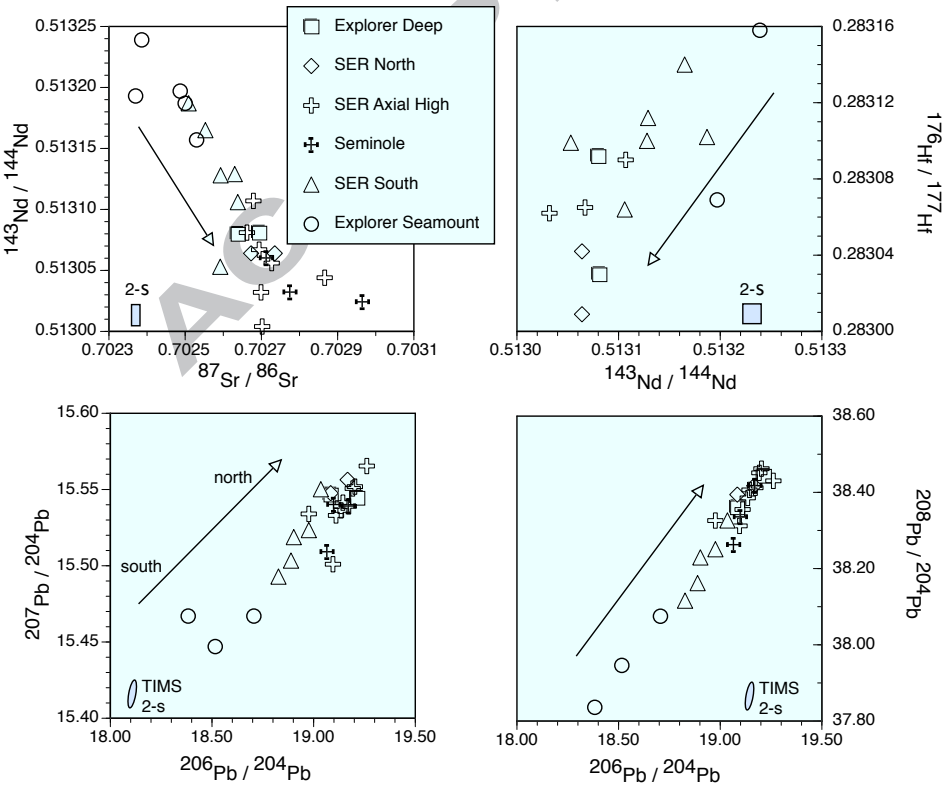

Figure 8

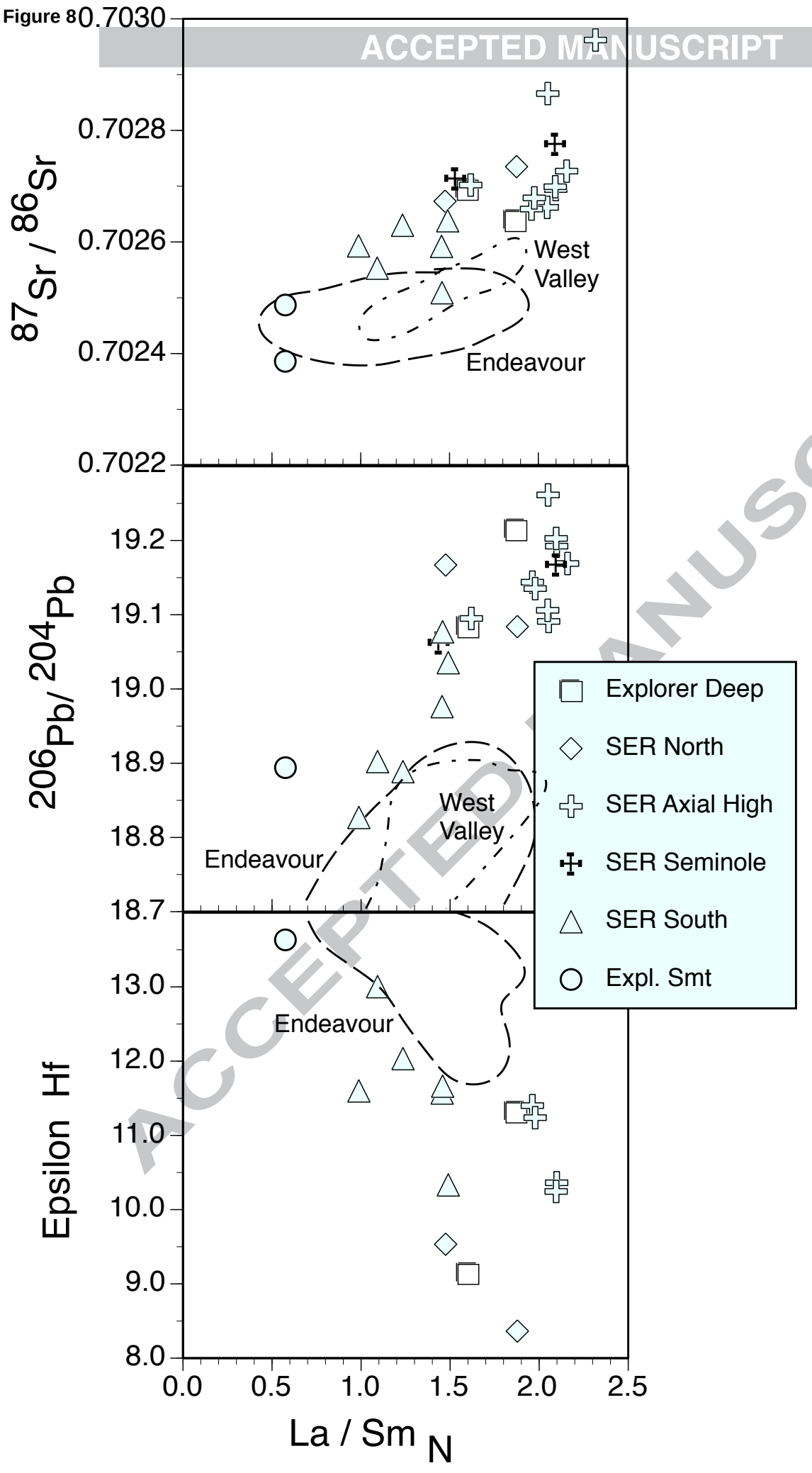

Figure 9



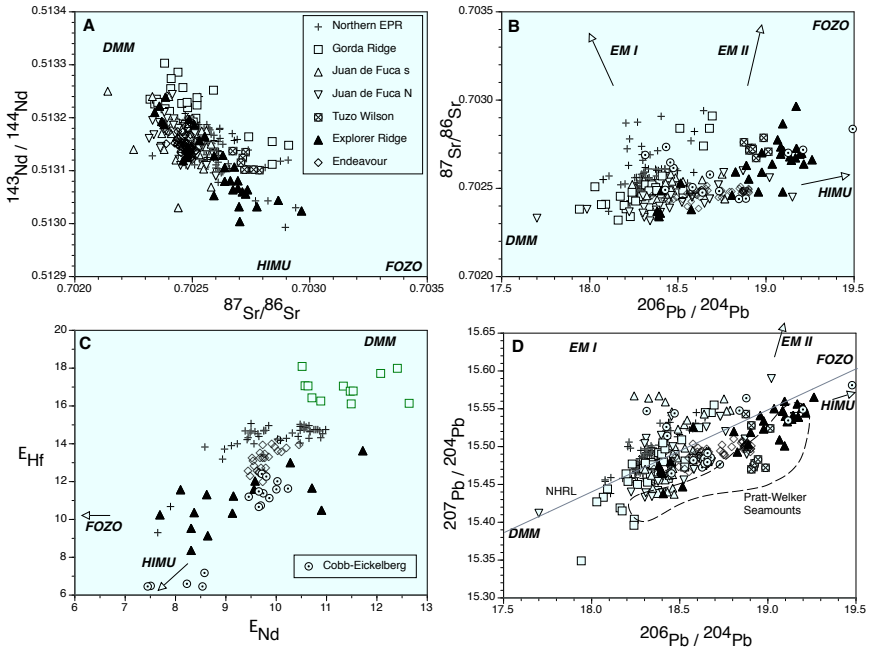

Figure 10



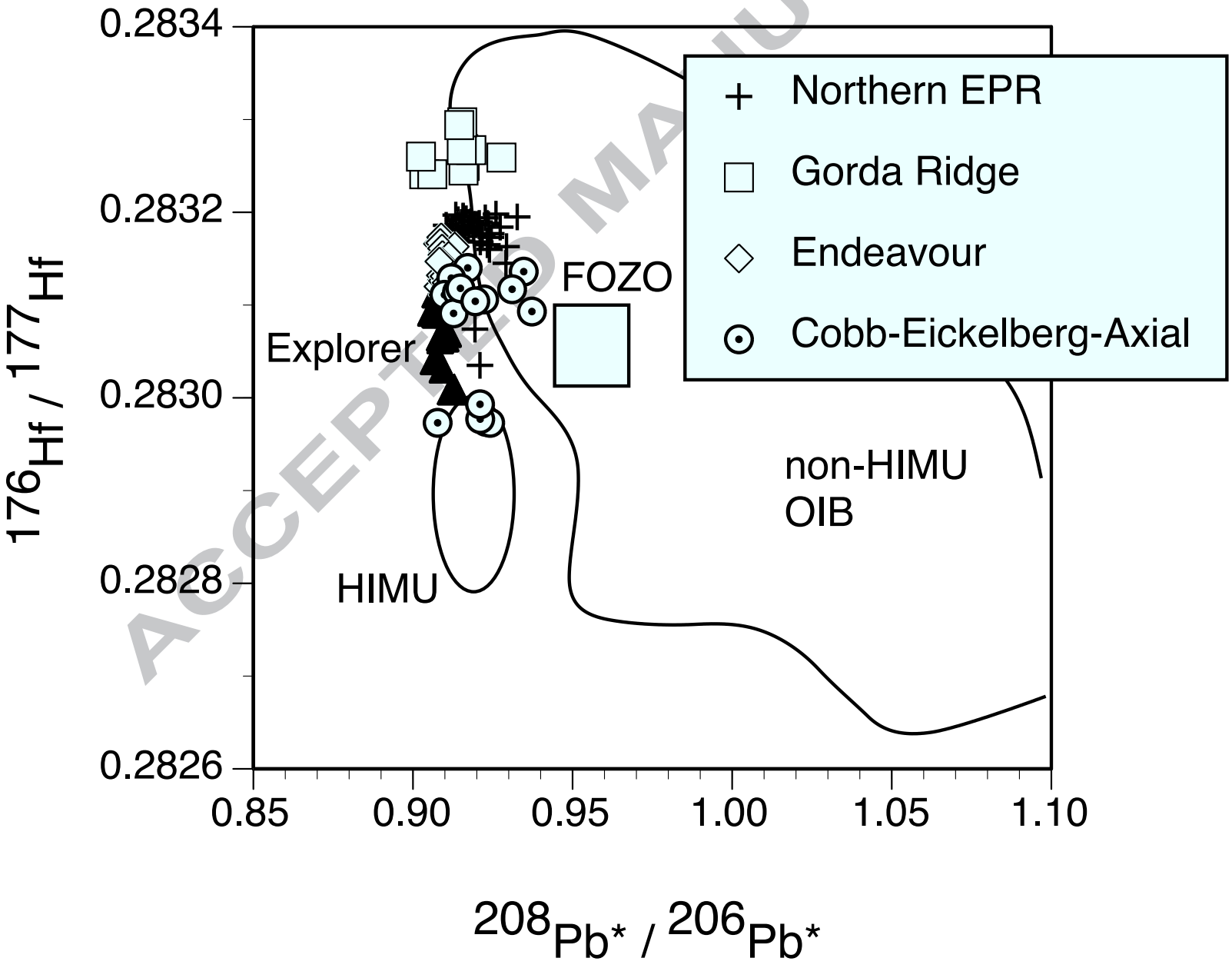

Figure 11